May 2017

Ash Tree Identification Based on the Integration of Hyperspectral Imagery and High-density Lidar Data

Haijian Liu
University of Wisconsin-Milwaukee

ASH TREE IDENTIFICATION BASED ON THE INTEGRATION OF HYPERSPECTRAL IMAGERY AND HIGH-DENSITY LIDAR DATA

by

Haijian Liu

A Dissertation Submitted in

Partial Fulfillment of the

Requirements for the Degree of

Doctor of Philosophy

in Geography

at

The University of Wisconsin-Milwaukee

May 2017

ABSTRACT
ASH TREE IDENTIFICATION BASED ON THE INTEGRATION OF HYPERSPECTRAL IMAGERY AND HIGH-DENSITY LIDAR DATA

by

Haijian Liu

The University of Wisconsin-Milwaukee, 2017
Under the Supervision of Professor Changshan Wu

Monitoring and management of ash trees has become particularly important in recent years due to the heightened risk of attack from the invasive pest, the emerald ash borer (EAB). However, distinguishing ash from other deciduous trees can be challenging. Both hyperspectral imagery and Light detection and ranging (LiDAR) data are two valuable data sources that are often used for tree species classification. Hyperspectral imagery measures detailed spectral reflectance related to the biochemical properties of vegetation, while LiDAR data measures the three-dimensional structure of tree crowns related to morphological characteristics. Thus, the accuracy of vegetation classification may be improved by combining both techniques. Therefore, the objective of this research is to integrate hyperspectral imagery and LiDAR data for improving ash tree identification. Specifically, the research aims include: 1) using LiDAR data for individual tree crowns segmentation; 2) using hyperspectral imagery for extraction of relative pure crown spectra; 3) fusing hyperspectral and LiDAR data for ash tree identification. It is expected that the classification accuracy of ash trees will be significantly improved with the integration of hyperspectral and LiDAR techniques.

Analysis results suggest that, first, 3D crown structures of individual trees can be reconstructed using a set of generalized geometric models which optimally matched LiDAR-

derived raster image, and crown widths can be further estimated using tree height and shape-related parameters as independent variables and ground measurement of crown widths as dependent variables. Second, with constrained linear spectral mixture analysis method, the fractions of all materials within a pixel can be extracted, and relative pure crown-scale spectra can be further calculated using illuminated-leaf fraction as weighting factors for tree species classification. Third, both crown shape index (SI) and coefficient of variation (CV) can be extracted from LiDAR data as invariant variables in tree's life cycle, and improve ash tree identification by integrating with pixel-weighted crown spectra.

Therefore, three major contributions of this research have been made in the field of tree species classification:1) the automatic estimation of individual tree crown width from LiDAR data by combining a generalized geometric model and a regression model, 2) the computation of relative pure crown-scale spectral reflectance using a pixel-weighting algorithm for tree species classification, 3) the fusion of shape-related structural features and pixel-weighted crown-scale spectral features for improving of ash tree identification.

Dedicated to my parents,

my wife,

my son,

and my daughter

TABLE OF CONTENTS

LIST OF FIGURES

LIST OF TABLES

ACKNOWLEGEMENTS

I would like to express my deepest thanks to my advisor, Professor Changshan WU. Without his sincere help, patient direction, and heartening encouragement, I would not possible finish my Ph.D work. His expertise and experience in remote sensing shared with me have positively influenced my research, and his suggestions and guidance will be a precious treasure in my lifetime. Special thanks also go to my committee members, Professor Alison Donnelly, Professor Zengwang Xu, Professor Lingqian Hu, and Professor Pingliang Dong from Uniersity of North Texas for their valuable suggestions on my dissertation work.

I also appreciate other faculty members in Geography department who helped me during my graduate study in UW-Milwaukee. Professor Glen Fredlund, Professor Ryan Holifield, Professor, Professor Kristin Sziarto, Professor Rina Ghose, Professor Hyejin Yoon, Professor Mick Day, and Ms. Donna Genzma. I also like to thank all the fellow graduate students in Geography UW-Milwaukee, Yingbin Deng, Wenliang Li, Yang Song, Hong Zhuo, Wei Xu, Feng Pan, Minji Kim, Gainbi Park, So Hyung Lim, Nicholas Schuelke, Nicholas Padilla, and Yui Hashimoto.

My final thanks to my parents, my wife Shan Gao, my son Patrick Liu, and my daughter Lucy Liu for their consistent support and encouragement.

CHAPTER 1 INTRODUCTION

1.1.Background

Urban forests, simply defined as tree-dominated vegetation in urban areas, have contributed to the sustainability of urban ecosystems, economic development, and urban life quality (Chen and Wang, 2013; Konijnendijk et al., 2006). Acting as carbon sinks in the earth's carbon cycle, urban forests help to mitigate climate change by removing carbon dioxide (CO_2) from the atmosphere via photosynthesis (Deng et al., 2011; Nguyen et al., 2015). In the United States, the carbon sequestered by urban forests in 2005 is estimated to be approximately 643 million tons, accounting for 14% of the total amount sequestered by the entire nation's forests (Godwin et al., 2015). Urban forests improve the liveability of cities by reducing storm-water runoff, improving air quality by removing air pollutant (e.g., PM 2.5), and ameliorating the heat-island effect by providing shade and releasing water into the atmosphere to keep it cool (Armson et al., 2012; Nguyen et al., 2015). Urban forests also play a critical role in reducing energy costs by reducing air conditioning needs and increasing property values (Mullaney et al., 2015).

As a popular street tree species, ash trees (*Fraxinus spp*) are widely planted due to their tolerance of a wide range of soil and climate conditions in many urban areas of the United States, especially in the eastern and middle parts of the country (Harlow, 1991; MacFarlane and Meyer, 2005). Ash is the common name given to various species belonging to the *Fraxinus* genus and includes white ash, green ash, and black ash, characterized by opposite and pinnately compound leaf arrangement (Harlow, 1991). Ash trees are cultivated for ecological, ornamental and commercial purposes, as the large crown is one of the top choices of road greening; the strong but elastic wood is used for tool handles; baseball bats and furniture products; and their fruit

provides food for various animals. They are abundant in many eastern central and western cities of the United States. In the City of Milwaukee, a Midwestern city of the United States, the ash tree population is estimated to be approximately 573,000 in 2008, accounting for 17.4% of urban tree canopy (Sivyer, 2010).

Ash trees are vulnerable to injury from exotic bark beetles like the emerald ash borer (*Agrilus planipennis* Fairmaire, EAB), which was introduced to North America from Asia in the 1990s and was first detected in metropolitan Detroit, Michigan in 2002 (Cappaert et al., 2005; Poland and McCullough, 2006). The EAB has spread across at least 18 states in America (Flower et al., 2013; Pugh et al., 2011) and killed tens of millions ash trees in the United States (*FAO,2013*). Kovacs et al. (2010) predicted the EAB infestation will expand to 25 states and the cost of treatment, removal, and replacement of over 17 million ash trees will reach $10.7 billion by 2019. Previous studies suggest all ash species in eastern North American are susceptible to EAB due to their related genetic properties (Herms et al., 2004; MacFarlane and Meyer, 2005). The key damage is produced by the larvae who feed on the inner bark of ash trees and disrupt the transportation of water and nutrients (Castrillo et al., 2008). After EAB infestation, mature ash trees will experience mortality within 3 to 5 years, but signs of EAB infestation is not obvious before visual symptoms occur, such as yellow leaves and dieback of fine twigs (Pontius et al., 2008). This indicates that it is not reliable to detect EAB infestation before it affects tree health. Therefore, identifying healthy ash trees in urban ecosystems is critical for ash tree management and planning (McKenney et al., 2012).

In comparison with time-consuming and laborious intensive ground-based inventories, remote sensing techniques provide an alternative mean to study urban trees with greater efficiency over large areas (Martin et al., 1998). Remote sensing records the electromagnetic

energy emitted or reflected from an object without making direct contact with it but permits certain physical properties to be determined. Remote sensors can be divided into two groups: passive and active. Passive sensors record natural energy reflected or emitted from the Earth's surface. In particular, the remote sensing systems recording energy over several separate wavelengths are referred to as multispectral sensors, whereas systems detecting over hundreds of very narrow spectral bands are called hyperspectral sensors. Multispectral imagery, such as Landsat Thematic Mapper (TM), have been widely used for mapping urban landscape heterogeneity at regional scale (Singh et al., 2012), classifying land cover at continental or national scales (Colditz et al., 2011), and evaluating multiple stages of tree mortality (Meddens et al., 2011). Hyperspectral imagery has the ability to improve land-use/land cover classification in comparison to multispectral images (Petropoulos et al., 2012a), and discriminate tree species in urban forests (Alonzo et al., 2013; Green et al., 1998), temperate forests (Heinzel and Koch, 2012), and tropical rainforests (Clark et al., 2005).

In contrast, active sensors project a laser onto the Earth's surface and record the backscattered energy. Light detection and ranging (LiDAR) is a promising and widely applied active remote sensing technology which can be used to segment individual trees (Koch et al., 2006), measure three-dimensional distribution of a forest canopy, and estimate other canopy parameters, such as tree position, tree height, crown diameter (Morsdorf et al., 2004), and biomass (Lefsky et al., 2002). Moreover, LiDAR derived features, such as signal intensity, crown texture, and canopy structure, offer complementary information for species discrimination. As a result, the integration of optical images and LiDAR data is capable of improving classification performance (Lu and Weng, 2007).

1.2 Literature review

Urban tree species identification remains a challenge due to the variability within a given species, spectral and spatial similarity among species, and high species diversity in urban environments (Alonzo et al., 2013). The common remote sensing data sources for tree species identification include LiDAR data, multispectral, and hyperspectral imagery. Among these three data sources, hyperspectral techniques have proven to be the most effective for tree species identification due to its ability to capture subtle differences in spectral signature (Martin et al., 1998). Multispectral imagery, with several discrete bands, has limitations in tree species classification due to the lack of required spectral range and resolution (Clark et al., 2005). Further, LiDAR data can measure three-dimensional tree properties, and is capable of detecting individual trees, segmenting forest canopy, and estimating single tree metrics. Thus, the integration of hyperspectral imagery and LiDAR data are reported to be beneficial for tree species classification (Zhang and Qiu, 2012).

1.2.1 Tree species classification with hyperspectral imagery

Hyperspectral imagery is characterized by hundreds of very narrow but contiguous spectral bands throughout the visible and infrared portions of the electromagnetic spectrum. The fine bands make it possible to measure pertinent discriminatory spectral features ranging from 400 to 2500 nm (Cochrane, 2000). Hyperspectral data can be acquired at the leaf-, pixel- and crown-scale, with different scale data recording spectral information at different levels. Tree species identification using hyperspectral imagery at the pixel and crown scales has been widely applied in urban forest, boreal forest, and tropical forest environments (Clark et al., 2005; Dalponte et al., 2013; Zhang and Qiu, 2012).

1.2.1.1 Reflectance properties at leaf, pixel, and crown scales

Leaf scale reflectance spectra are usually measured by a hand held spectrometer in a controlled laboratory environment which results in a relatively high ratio of signal to noise (Clark et al., 2005). Leaf spectra variability is mainly determined by leaf biochemical properties (e.g., chlorophyll content, water, pigments) and morphology (e.g., air spaces, cuticle wax, mesophyll). Spectral variability in the visible range among species is low due to strong absorption by chlorophyll while transmittance and reflectance in the near infrared range is high due to photon scattering within the spongy mesophyll. Clark et al. (2005) found the leaf spectral variability among the seven emergent species in a tropical rain forest was significantly greater than that within species, and these species have been discriminated using leaf-scale reflectance with >89% overall accuracy. In particular, leaf-scale classification using the Linear Discriminant Analysis (LDA) approach and 40 optimally selected bands had 100% overall accuracy (Clark et al., 2005). Shang and Chisholm (2014) achieved the best result for six eucalyptus species and one non-eucalyptus species classification at the leaf level when compared to crown- and community-level classifications. Similarly, Xiao et al. (2004) mapped 22 tree species with 94% accuracy at the leaf-level in Modesto, California.

Pixel-scale reflectance spectra are usually measured by airborne or spaceborne sensors. For trees, the shapes of pixel-scale reflectance spectra are generally similar to those of leaf-scale spectra, but the overall reflectance is low due to the effects of fine-scale shadows within leaves and branches (Clark et al., 2005). Pixel size also affects the spectral signature. Fine spatial resolution can partially address the mixed-pixel problem, but generally with issues of shadows (Lu and Weng, 2007).

Crown-level (or tree-level) reflectance spectra are the aggregation of pixel spectra within a crown. For crown-level analysis, crown segmentation is generally conducted to cluster spectrally similar and spatially proximate pixels into crowns, and the resultant crown-level spectra are derived as the average of the spectra of individual pixels within the crown (Alonzo et al., 2014). In particular, Clark et al. (2005) averaged all the pixels' spectra in a crown to create the crown-level reflectance spectra. Dalponte et al. (2013) extracted the spectra at crown level using a pixel majority method. Further, Zhang and Qiu (2012) selected the spectra of the pixel at the treetop to represent the spectra of a crown.

1.2.1.2 Tree species classification

For tree species' classification, normalized difference vegetation index (NDVI) derived from hyperspectral imagery has been employed to identify vegetation and non-vegetation or identifying different vegetation species (Xiao et al., 2004). A simple NDVI threshold method can differentiate the tree canopy spectra from the confounding spectral noise from other materials (Alonzo et al., 2013). However, the simple method cannot capture the unique spectral feature of specific tree species.

As a better alternative, hyperspectral imagery has been widely used for tree species classification. Ustin and Xiao (2001) proved that the classification accuracy of vegetation can be improved with hyperspectral airborne visible/Infrared imaging Spectrometer (AVIRIS) imagery, when compared to the three-band SPOT imagery at the same spatial resolution. Further, Xiao et al. (2004) separated conifers, broadleaf deciduous, and broadleaf evergreen with the average accuracy of 94%, 99%, and 83% using hyperspectral imagery. This satisfactory classification accuracy is primarily due to the clear difference among their spectra: conifers have the lowest reflectance values; broadleaf deciduous have the highest reflectance values; and the reflectance

6

values of broadleaf evergreens are in the middle. Furthermore, Gong et al. (1997) confirmed the potential of hyperspectral data in separating six conifer species with an accuracy of 70% or higher. Dalponte et al. (2009) distinguished 23 broadleaf species in Mediterranean environments and obtained high accuracy (over 90%) for certain species. In addition, foliar chemistry derived from hyperspectral data can be used to classify species composition. Martin et al. (1998) identified 11 species compositions with an overall classification accuracy of 75% by combining two chemical compositions: nitrogen and lignin concentration in forest canopy foliage.

For tree species classification, pixel-level classifications, which assign a pre-defined class to each individual pixel and provide qualitative assessment of tree species distributions, are often carried out. Pixel-level classifications can be achieved through employing supervised or unsupervised classifiers. In particular, George et al. (2014) applied supervised Support Vector Machines (SVM) and Spectral Angle Mapper (SAM) classifiers to EO-1 Hyperion imagery for discriminating and classifying six broadleaved evergreen and conifer tree species, and resulted in an overall accuracy of 82.27% with kappa statistic of 0.79 for broadleaved evergreen and overall accuracy of 74.68% with kappa statistics of 0.70 for conifers. Petropoulos et al. (2012a) combined Hyperion hyperspectral imagery with supervised SVM and Artificial Neural Networks (ANN) to classify ten land cover types. Dalponte et al. (2013) evaluated VNIR and SWIR hyperspectral data with SVM, random forest (RF), and Gaussian maximum likelihood (GML) classifiers in discriminating four boreal species at the pixel level. The combination of VNIR and SWIR results in a similar accuracy as VNIR alone, but higher accuracy was reported with VNIR when compared to SWIR. In addition, SVM classifier was reported as a better approach when compared to RF and GML classifiers, primarily due to its insensitivity to the feature selections. With per-pixel classifications, the mixed pixels have been recognized as a problem that affects

the applications of remotely sensed data in species classification (Lu and Weng, 2004). In addition, the "salt and pepper" effect may also reduce the classification accuracy (Yu et al., 2006).

Subpixel classification approaches improve land cover classifications when compared to per-pixel approaches, especially when dealing with mixed pixels (Lu and Weng, 2007). Sub-pixel classification extracts the proportion of individual materials of interest within a pixel and results in a more discriminated classification than traditional per-pixel classifiers. Spectral mixture analysis (SMA) is a popular and effective method to derive the subpixel information from remotely sensed imagery. Bai et al. (2012) employed a linear SMA to improve the estimation of three forest covers in a complex subtropical forest. Lu and Weng (2004) developed a new conceptual model to characterize urban landscape patterns using linear SMA. With five endmembers: shade, green vegetation, impervious surface, dry soil, and dark soil, the minimum noise fraction (MNF) transformed components were un-mixed into fraction images using an unconstrained least-squares solution. Wu (2004) developed a normalized spectral mixture analysis (NSMA) method to examine urban compositions. Somers et al. (2010) applied a weighted multiple endmember Spectral Mixture Analysis (wMESMA) to monitor the level of defoliation of Eucalyptus. Both NSMA and MESMA reduced endmember variability in spectral data and improved the results as compared to simple SMA. Somers et al. (2007) presented a nonlinear hyperspectral mixture for tree cover estimates which considered the multiple photo scattering among different surface components. The nonlinear spectral mixture analysis reduced the estimation error but the virtual fractions do not have physical meanings.

Crown-level classification is increasingly demanded for providing a quantitative estimation of tree species (Dalponte et al., 2013), from which, the forest variables, such as number, volume,

and height of any species can be extracted, so crown-level classification has enhanced our ability to make a practical map in forest inventories. Several methods were developed for species classification at the crown-level. Clark et al. (2005) discriminated seven tropical rainforest tree species using the mean spectra from manually-delineated crown and obtained a crown-level classification accuracy of 90%, higher than pixel-level accuracy (85%). Dalponte et al. (2013) aggregated the pixels within the manually defined tree crowns and assign the tree species corresponding to the majority of the pixels in classifying Pine, Spruce, Birch, and other species in boreal forests. Alonzo et al. (2013) extracted all spectra exceeding an NDVI threshold of 0.6 from AVIRIS imagery and mapped 15 urban tree species using the pixel majority approach, and resulted in an overall accuracy of 86% in classifying 15 common urban trees in Santa Barbara, California, United States. Xiao et al. (2014) achieved 70% accuracy in mapping 22 urban tree species in Modesto, CA, Unites States, and the crown-level spectra were extracted using multi-masks based on the NDVI threshold and spectral mixture analysis (SMA) analysis with AVIRIS data. Zhang and Qiu (2012) developed a treetop-based classification at the crown level and achieved the overall classification accuracy of 69% in mapping 40 tree species using hyperspectral imagery in an urban forest in north Dallas, Texas, United States. The treetop based classification only analyzes the hyperspectral pixel at the highest point per crown and assigns the identified species type of the treetop pixel to the entire tree crown, which reduces the influence from shadows, gaps, double-sided illuminations, and mixed pixel problems.

1.2.2   Identification of individual tree crowns using LiDAR data

Identification of individual tree crowns has a significant implication in forest inventories and management (Chen et al., 2006; Wu et al., 2016). In comparison with passive imaging, the discrete LiDAR has the advantage of characterizing the 3-dimensioanl (3D) structure of forests

9

as it generates 3D point data with high spatial resolution (Li et al., 2012), and therefore identify

individual tree crowns with high accuracy and efficiency (Hu et al., 2014). Specifically, the

transmitter system of LiDAR emits pulses of laser light ranging from 1040 nm to 1060 nm to a

distant target on the ground at rates >100,000 pulses per sec. The LiDAR receiver system records

the laser energy backscattered from the target (Charaniya et al., 2004). The laser horizontal

position is recorded by the Global Position System (GPS) on the aircraft and the vertical height is

obtained by converting the travel time from the energy pulse transmission to reception into

distance (Popescu, 2007). LiDAR is classified as waveform and discrete-return systems (Lefsky

et al., 2002). The waveform LiDAR measures the vertical vegetation profiles by digitizing the

continuous reflected energy while the discrete-return LiDAR records either single or multiple

returns at precisely referenced points in time and space (Gatziolis and Andersen, 2008).

Compared with profiling LiDAR instruments, which are suitable for large-area forest

characterization in means of sampling, the discrete-return LiDAR from airborne laser scanning

systems are more commonly used for individual tree segmentation and structural information

extraction (Li et al., 2012; Wulder et al., 2012).

In areas with dense vegetation cover, LiDAR point cloud includes first returns from the

forest canopy and last returns from the ground (Lim et al., 2003). Therefore the digital surface

model (DSM) and the digital elevation model (DEM) can be created by interpolating the first and

last returns to represent surface elevation and bare terrain elevation above sea level respectively.

And further, the canopy height model (CHM), characterizing canopy height, can be created by

subtracting the DEM from the DSM (Popescu, 2007). However, the CHM derived from the raw

LiDAR data often exhibits many holes due to data acquisition and post-processing, which leads

to inaccurate biophysical measurement, average tree height underestimation, and errors in

estimating forest biomass (Ben-Arie et al., 2009).   Therefore, it is imperative to fill the pits to

obtain an accurate CHM for individual tree delineation and tree height estimation (Leckie et al.,

2003; Popescu and Wynne, 2004). Verma and Kumar (2011) designed a low-pass filter to

replace the highest or lowest value within a neighborhood by its median value. The filter can

make the canopy smooth but also changes the canopy shape to some degree. Leckie et al. (2003)

proposed a pre-processing attempt to remove the holes, which overlaid the 3D point cloud with a

25 cm grid and created the DSM by interpolating the highest point in each grid. The peak-based

interpolation reduces the number of pits but some still remained. Ben-Arie et al. (2009)

presented a semi-automated algorithm to fill the holes from CHM, which detected the data pits

by a user-defined threshold and fill them with the neighborhood value. The approach

outperforms median, mean and Gaussian smoothing filters but it relies on users' experience.

Based on forest structural characteristics, a variety of techniques were developed to detect the

individual tree crowns using discrete LiDAR data, such as valley following, edge finding,

clustering, radiance peak filtering, and template matching (Wulder et al., 2000). Typically, the

processes of identifying single trees include two major steps: treetop detection and crown

delineation.

Treetop detection is the basis for tree height extraction, crown delineation, and further tree

species classification (Koch et al., 2006). Local maximum (LM) technique provides a way to

locate treetops based on the assumption that the highest laser value in a spatial neighborhood

represents the tip of a tree crown (Popescu, 2007; Popescu et al., 2003; Wulder et al., 2000).

Popescu and Wynne (2004) operated the LM filtering with two shaped search windows: a square

n by n window and a circular window on the CHM to detect treetops. The results indicated the

circular window with variable size outperformed the static-size square window. Chen et al.

(2006) applied the LM filtering on a LiDAR-derived canopy maxima model (CMM) rather than the CHM to detect the treetops in a savanna woodland. With variable windows determined by the lower-limit of the prediction intervals of the regression model, the new method resulted in higher accuracy for tree isolation (54.4%) than the method with CHM (37.0%). Besides the LM filtering technique, Persson et al. (2002b) developed a climbing method to search for local height maxima in the smoothed image. The method allows every pixel to climb in the direction of the largest slop to reach a local maximum where all neighboring pixels had lower values, and further estimates the crown coverage by grouping those pixels that climbed to the same maximum.

The correct crown delineation is a prerequisite for crown structural metric extraction, crown volume estimation, and tree species identification (Alonzo et al., 2014; KOCH et al., 2002). Several methods have been explored to segment individual trees within a forested region. Leckie et al. (2003) applied a valley following approach to a digital height model for individual tree isolation. The valley following approach was proposed by Gougeon (1995) to automatically delineated individual tree crowns in high spatial resolution aerial images. The potential tree crowns were masked out by a valley following procedure from the local minima and crown boundaries were detected by a rule-based approach. The crown isolation obtained using the valley following approach on CHM matched 75% of the ground reference trees. Chen et al. (2006) proposed a marker-controlled watershed segmentation into isolating individual trees in savanna woodland. The treetops were located as markers to improve accuracy and watershed ridge lines were detected to divide adjacent catchment basins in the image. Koch et al. (2006) developed a pouring algorithm to delineate tree crowns with a small footprint LiDAR data in deciduous and mixed temperate forests. Resembling water being poured onto mountains, crown regions extended from the local maxima to lower height values. The final crown regions were

obtained by merging very small segments or disjoining the tree groups with knowledge-based assumptions on the shape of trees. Besides LiDAR-derived CHMs, Liu et al. (2013) directly segmented individual trees from airborne LiDAR point clouds in human settlements. In the process of extraction, the LiDAR point clouds were first segmented into point clusters by a surface growing algorithm, the tree points were then distinguished based on their multiple echo properties, and the accurate edges of each tree was extracted by employing the spoke wheel algorithm. Experiments showed more than 85% of trees were extracted with accuracy higher than 95%.

1.2.3 Extraction of crown structural features from LiDAR data

LiDAR data has played an important role in forestry applications (Heinzel and Koch, 2012). Based on isolated individual trees, the most important geometric properties including tree height and position can be directly derived (Popescu et al., 2002). Other properties including crown diameter and crown volume can be calculated (Morsdorf et al., 2003), and the specific tree species can be distinguished (Koch et al., 2006). Popescu and Wynne (2004) applied the LM filtering to measure the individual tree height on CHM and concluded the best LiDAR measurements explained 97 percent and 79 percent of mean height variance for dominant trees on pine plots and deciduous plots respectively. Persson et al. (2002b) evaluated the accuracy of the tree height estimation using an airborne laser scanner in southern Sweden and small error of tree height measurements of the detected sample trees (0.63 m) was reported. Wang and Glenn (2008) designed a new linear regression method for tree canopy height estimation using LiDAR data. Results indicated the method produced more accurate tree canopy heights in comparison with the traditional local maximum filtering and multiple regression methods.

Crown size is another critical factor in determining canopy cover and associating tree species classification (Biging and Dobbertin, 1995). Popescu et al. (2003) developed a four-degree polynomial to fit two perpendicular profiles from the location of each tree top on the CHM, and calculated the individual crown diameter as the average of two values measured along two profiles. The accuracies of estimating crown diameters for pines and deciduous trees were similar with R^2 values of 0.62-0.63. Persson et al. (2002b) applied the hill climbing method to group pixels into segments for crown segmentation. The area of the segments was used to calculate the crown diameter by assuming the tree crown had the shape of a circle and resulted in a root-mean-square error (RMSE) of 0.61 m. Moreover, Kato et al. (2009) developed a wrapped surface method to capture tree crown formation using airborne LiDAR data, and the crown width was derived with an R^2 value of 0.8.

LiDAR data points have the ability to measure the three-dimensional (3-D) position of tree elements, thus the foliage distribution and branching patterns can be extracted from LiDAR point cloud for improving forest species classification. Li et al. (2013) derived a set of horizontal and vertical structures including 3-D texture, foliage clustering degree, foliage clustering scale, and gap distribution of individual trees from LiDAR data, and successfully classified four species with an overall accuracy of 77.5% by combining linear discriminant analysis and these structural features. Ørka et al. (2009) discriminated coniferous and deciduous tree species using laser height distribution and intensity features derived from airborne laser scanner data. The structure and intensity features resulted in 77% and 73% overall accuracy respectively, while the combination of them classified the species with an overall classification accuracy of 88%. The geometric properties of the object can also be measured by a 3-D shape signature, a probability distribution sampled from a shape function measuring a 3-D object. With the shape signature,

the 3-D shape matching problem can be reduced to the comparison of 2-D probability distribution. Osada et al. (2002) proposed five shape functions, including A3, D1, D2, D3, D4, to compute 3D shape signature and Dong (2009) applied D2, measuring the distance distribution of random point pairs, to characterize Oak and Douglas fir and successfully distinguish them at the individual tree level.

1.2.4 Integration of Lidar data and hyperspectral images

Hyperspectral imagery has been employed as the primary data source for classifying urban tree species (Dalponte et al., 2012), but confusion occurs with similar spectral properties of different tree species (Liu et al., 2011). Comparatively, LiDAR data can provide a set of crown structural variables, such as tree height, crown base height, and LAI for tree classification, but LiDAR alone is not sufficient for species discrimination among large numbers of species (Alonzo et al., 2014). As a result, fusion of these two data sources may benefit tree species classification due to the integration of crown structural and biochemical information. In remote sensing literature, fusion is a common term which refers to the integration of multisensor data at the pixel, feature, or decision levels (Pohl and Van Genderen, 1998). To date, fusion of LiDAR and hyperspectral data are promising for tree species classification (Alonzo et al., 2014). Zhang and Qiu (2012) explored a simple integration of hyperspectral imagery and LiDAR data in northern Dallas, Texas. LiDAR data was used for treetop identification and tree crown delineation, and the hyperspectral features of the crowns were extracted for species classification. Results showed that 93.5% of trees were detected from LiDAR data and 69% of tree species were identified from hyperspectral imagery.

Fusion at the pixel level adds LiDAR derived structure information into spectral bands. Jones et al. (2010) integrated the height and volumetric information derived from LiDAR with

hyperspectral Airborne Imaging Spectrometer for Applications (AISA) imagery for 11 tree species maps in coastal South-western Canada. The fusion resulted in an increase of producer's accuracy (5.1-11.6%) and user's accuracy (8.4-18.8%). Dalponte et al. (2008) directly added two LiDAR derived elevation and intensity information into the 126 bands of hyperspectral imagery and found that, with the LiDAR data, the classification accuracy for 5 classes (out 23) improved more than 5%. The in-depth fusion at the crown level integrates more spectral and spatial characteristics of tree crowns to improve the accuracy of tree species classification. Dalponte et al. (2012) selected 6 (out of 19) LiDAR features and 43 (out of 126) spectral features for seven tree species classification. The experimental results showed that the LiDAR contribution reached 10% when combined with hyperspectral imagery, and the high density LiDAR data outperformed low density data due to the ability of additional feature extractions. Alonzo et al. (2014) fused high-spatial resolution (3.7 m) hyperspectral imagery and high-density (22 pulse/m^2) LiDAR data to map 29 common species in Santa Barbara, California, US. For each crown, 28 structural metrics were fused with multi-spectra of pixels which exceeded an NDVI threshold of 0.6. The addition of LiDAR data resulted in a 4.2% increase of overall classification accuracy and an over 40% increase for small or morphologically unique crowns than hyperspectral data alone.

In general, hyperspectral data has the ability to measure subtle variations in the reflectance of plants due to their narrow bandwidth and wide range of electromagnetic spectrum. The spectral reflectance, however, is influenced by other objects (e.g. branches, shades, etc.) even after radiometric calibration and atmospheric correction. As a result, the overall accuracy of the classification with hyperspectral imagery at crown level was proven to be lower than that at leaf level (Clark et al., 2005). On the other hand, LiDAR data offers complementary information to

optical data for tree species identifications (Alonzo et al., 2014; Dalponte et al., 2008; Zhang and Qiu, 2012). With detailed and accurate point coverages of LiDAR data, single tree delineation in forest stands can be reached (Brandtberg, 1999; Hyyppä and Inkinen, 1999), and individual structural features, including tree heights, crown sizes, and crown shape signature, can be extracted (Dong, 2009; Hyyppä et al., 2000; Popescu et al., 2002).Therefore, the fusion of hyperspectral and LiDAR data has the capability to improve species classification accuracy.

1.3 Problems statement

Ash accounts for a large proportion of trees in Milwaukee, and most of them are at risk of attack from EAB. Therefore, rapid detection of ash trees using remote sensing could benefit Milwaukee planners in determining the distribution of ash trees in the city and thereby help implement a protection program. This research focuses on the integration of hyperspectral imagery and LiDAR data for improving the accuracy of crown-level ash tree identification.

Crown-level tree species classification is increasingly demanded due to the ability of providing quantitative estimation of tree species, but the performance of the species classification is affected by the performance of individual tree crown identification. Although manual delineations of tree crowns could result in high classification accuracies, it is time-consuming and is limited to user experience (Clark et al., 2005; Dalponte et al., 2013). The treetop-based classification avoids the impacts from crown delineation errors, but the spectral signature of a tree extracted from only the treetop is sensitive to the accuracy of the treetop detection and the spectral purity of the treetop pixel (Zhang and Qiu, 2012). In addition, the ambiguous crown boundaries on aerial photos or canopy height model decrease the accuracy of crown delineation, and further negatively impact the structural feature extraction and tree species

classification (Van Leeuwen et al., 2010). In conclusion, accurate identification of individual tree crowns using LiDAR data has become challenging work.

Crown-scale spectra can be calculated by averaging all the pixel spectra or the pixel spectra exceeding a specific threshold within a crown (Clark et al., 2005). However, the technique of linear averaging within-crown pixel spectra ignores the impact of the mixed-pixel problem and double-side illumination problem (Sinha et al., 2012). In complex forests, trees may intertwine and overlap, branches of leaves may cast shadows, and the architecture of canopies may create a patterning of gaps (Jonckheere et al., 2004; Noest, 1994). Therefore, the pixels within a crown may subsume background plant species, soil and shadows, and thereby produce mixed crown-scale spectra (Clark et al., 2005). Due to the lack of purity of crown-scale spectra, low classification accuracy was observed (Gougeon et al., 1999). To minimize the classification error caused by pixel-mixed problems and double-side illumination problems, the generation of pure crown-scale spectra, with which the interfaces of non-photosynthetic vegetation and shadows were removed, becomes essential.

Crown structural features extracted from LiDAR data can provide complimentary information to hyperspectral imagery for improving tree species classification. However, the contribution of the LiDAR data is dependent on the selection of structural features. For example, individual tree height information is limited in singularly dominant age trees. Crown volume information has less explanatory power in multi-structured species classes (Jones et al., 2010). LiDAR intensity data may contain much noise from various sources and have low separability depending on the reflectance properties of surface materials (Song et al., 2002). Other structural features, such as crown height, crown widths at selected heights, and ratios of crown heights to width at selected heights, may contribute to the crown-scale tree species classification, but the

magnitude of them varies and there is no standard rule for metric selection (Alonzo et al., 2014). To maximize the contribution of LiDAR data and simplify the metric selection, the extraction of the structural features beyond the impacts of the age, architecture, and environment becomes more significant.

To identify ash trees, specific objectives of this proposed research include: (1) Using LiDAR data for individual tree crown identification; (2) Using hyperspectral imagery for crown-scale spectra extraction; (3) Extracting shape-related crown structural features from LiDAR data and fusing them with crown-scale spectra computed from hyperspectral imagery for ash tree identification.

CHAPTER 2 TREE CROWN WIDTH ESTIMATION USING DISCRETE AIRBORNE LIDAR DATA

2.1 Introduction

Light detection and ranging (LiDAR) is a promising technology for extracting forest biophysical parameters (Koch et al., 2006; Zhao et al., 2013). As an active remote sensing technology, the LiDAR system emits laser pulses to target objects and records the returned energy. The recorded energy from LiDAR includes the pulses reflected from the top of forest canopy, as well as those penetrating the top layer of the canopy to the ground, thereby resulting in 3-dimensional point clouds (Popescu, 2007). Once these raw points are filtered and classified into first and last returns, a digital surface model (DSM) and a digital elevation model (DEM) can be derived, respectively, and a canopy height model (CHM) can be obtained through subtracting DEM from DSM to characterize forest canopy structures. The unique characteristics of LiDAR, such as high sampling intensity, precise geolocation, accurate elevation measurement, and extensive areal coverage, make it essential for forest parameters estimation (Nilsson, 1996; Persson et al., 2002a; Popescu et al., 2003; Tao et al., 2014).

Early LiDAR studies of forest characteristics estimation emphasized on the plot level due to its easiness of data processing, broad-scale coverage, and relatively low cost (Bishop et al., 2014). Naesset (1997) measured mean tree heights of forest stands in a plot by averaging airborne laser height in user-defined grid cells. Similarly, Næsset and Økland (2002) estimated the ratio between the height measured from the ground surface to the crown base and that measured from the crown base to the top of trees at the plot level. In addition to height estimation, Maclean and Krabill (1986) and Holmgren et al. (2003) estimated the standing timber volumes of a plot through regressing against the cross-sectional area of the plot. Clark et al.

(2011) calculated the tropical rain forest aboveground biomass from plot vertical height profiles. Although forest biophysical parameters, such as mean height, volume, and biomass, have been successfully derived at the plot level, stem distributions cannot be generated (Yu et al., 2010), which prohibit the identification of tree species.

To address this problem, a large number of studies have recently applied LiDAR technology to measure forest biophysical parameters at the individual tree level. Popescu et al. (2002) detected individual tree positions using a local maximum (LM) filter and estimated tree heights based on the single tree identification. Koch et al. (2006) delineated tree crowns in deciduous and mixed temperate forests by employing a knowledge-based pouring algorithm. Popescu (2007) estimated diameter at breast height (DBH), and assessed aboveground and component biomass of individual trees using linear and non-linear regression methods. Moreover, accurate tree parameters were measured by reconstructing the crown model. Van Leeuwen et al. (2010) developed a new parametric height model (PHM) to describe the shape of forest canopy, through which a series of cones were created to fit the raw LiDAR cloud in order to represent individual trees. Sheng et al. (2001) developed a hemiellipsoid model to reconstruct conifer-crown surface. Moreover, crown shape parameters at the individual tree level (Dong, 2009) and tree species (Li et al., 2013) have been successfully extracted, using LiDAR data.

Despite the intense research efforts on forest biophysical parameters estimation, tree crown width estimation at the individual level, using LiDAR data, is challenging due to overlapping crown surfaces in urban forests (Popescu, 2007). Crown width, however, plays a critical role in determining canopy cover, calculating completion measures (Biging and Dobbertin, 1995), and estimating DBH, total volume, and biomass (Popescu, 2007; Popescu et al., 2003). In previous studies, crown width was usually estimated from other measurements. For example, Popescu et

al. (2000) indirectly computed average crown width with canopy closure and stand. Gill et al. (2000) estimated tree crown radius for several conifer species through developing linear and non-linear regression models. With these models, forest inventory variables such as DBH, tree height, and tree density were considered as independent variables. Further, Popescu et al. (2003) calculated individual crown diameters through employing the CHM. Specifically, crown diameters were calculated as the average distance between critical point along the 2 perpendicular profiles centered on the identified treetop, and the regression analysis suggested that the correlation coefficients between the estimated and reference diameters are approximately 0.62-0.63.

This article discusses the development of an innovative approach to automatically extract tree crown width in an urban area through integrating generalized geometric models with the regression models. Specific aims of the work are: (1) to develop a generalized geometric model to optimally fit different crown surfaces such as conical, hemisphere, and half ellipsoid; and (2) to develop a linear regression model to predict crown width based on tree height and crown shape.

2.2Study area and data

2.2.1   Study Area

Two census blocks (216m x 206m), located in the southeastern part of the University of Wisconsin-Milwaukee, located in Milwaukee, Wisconsin, United States, were selected as the study site (Figure 1). Ground surface in the study area is flat, and the average elevation of the site is about 200 m above sea level. This area is dominated by ash trees (*Fraxinus* spp.), maples

(*Acer* spp.), and oak (*Quercus* spp.). Several pines can also be found in the study area. The heights of trees along the roads are approximately 5 to 25 m. Field measurements were operated and LiDAR data were collected over the study site.
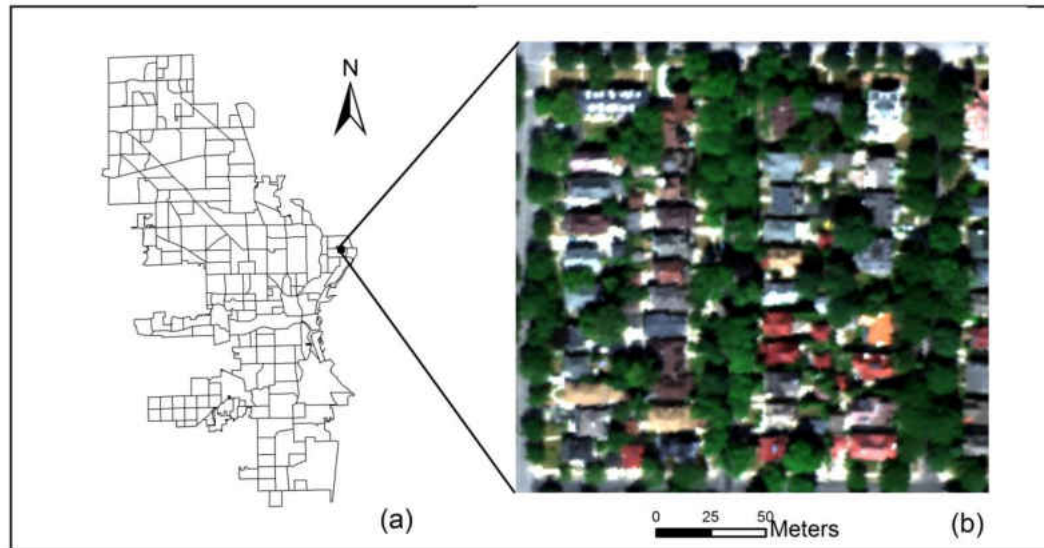
Figure 1 (a) Location and (b) hyperspectral imagery of the study area in Milwaukee, Wisconsin, United States.

2.2.2 Dataset

Both LiDAR and hyperspectral imager (HSI) data were collected by a team of Native Communities Development Corp (NCDC) imaging and RFP Mapping LLC, simultaneously, in August 2008. The initial data were processed by Terra Remote Sensing and the University of Victoria. As a result, LiDAR data were provided in a commonly used binary LASer (LAS) lidar format with State Plane coordinate system of Wisconsin South (FIPS 4803) and North American Datum of 1927 (NAD27). The average point density is 4 points/ m^2-5 points/m^2. HSI imagery has 366 bands with a spectral resolution of 4.7 nm and a spatial resolution of 1.0 meter. This image was projected to the Universal Transverse Mercator (UTM) coordinate system (Zone 16N)

with a datum of North American Datum of 1983 (NAD83). In addition to LiDAR and HSI, field data of the 135 trees identified from the LiDAR derived CHM were collected in November 2014. Crown widths of the trees along the road were measured by a distance tape in the field, and the trees' crown widths inside private properties were carefully measured on high resolution HSI and were rectified using the Google Earth map. The crown radii were measured in 4 perpendicular directions with a tape from tree trunk to the edge. Then, the crown width was calculated as the average of the 4 radii. The field measurement of crown width was used to generate the linear regression model as dependent variables for crown size prediction.

2.3 Data preprocessing

2.3.1 LiDAR data filtering

Because LiDAR data records returns from tree crown surface and the layers within them, the resultant raster image interpolated from the raw LiDAR data contains a lot of pits (as shown in Figure 2a), which adversely affecting the identification of crown shapes. Therefore, we employed the treetop height difference (THD) method developed by Liu and Dong (2014) to remove the first returned points under the crown surface. Following the THD method, the higher 30% of points in the circle filter window (r=1 m) were retained. With elevation attributes of the filtered LiDAR points and last return points, a DSM and a DEM were created, using the inverse distance weighting interpolation method. Further, the object height model (OHM) representing the height of tree canopy and other objects such as building was obtained by subtracting the DEM from the DSM. The smoothed image (Figure 2b) with spatial resolution of 0.2 m has a better representation of the real crown shape when compared with the original image (Figure 2a).
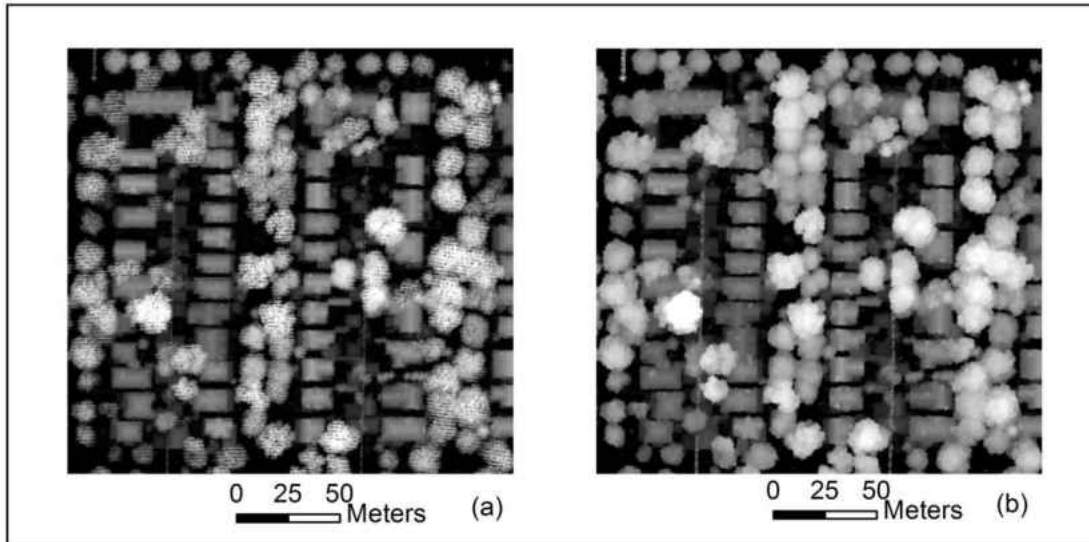
Figure 2 OHMs from the (a) original LiDAR data and (b) filtered LiDAR data.

2.3.2 Tree location detection

For a better identification of tree locations, we employed the normalized difference vegetation index (NDVI), calculated by using the aerial image spectral bands to separate trees from other features. In order to make the consistent coordinate system, the HSI was registered to the gridded LiDAR data (0.2 m spatial resolution). A total of 60 control points, evenly distributed across the study area, were derived from the OHM to geometrically reference the AISA imagery. Well defined corners of buildings and intersections of roads were selected because they are not likely to change over time and can be clearly found on both sets of data. After coregistration, the average root mean square error (RMSE) was approximately 0.2 pixels. With the AISA imagery, the average NDVI values of manually identified trees (0.68) and other features (0.12) were calculated, and the mean value of 0.4 was set as the threshold to separate trees and other features. This threshold is also consistent with the results reported in previous studies (Cristiano et al., 2014). When the NDVI value of a pixel on the OHM image is equal or less than 0.4, the spectral value of the corresponding pixel was recorded to no value. Through

applying the NDVI criterion method, other features such as roads and houses were removed from the LiDAR raster image and a CHM was created to map tree height (see Figure 3a). With this vegetation-only raster layer, local maxima points were detected using a 2 m × 2 m moving window to identify potential locations of treetops (see Figure 3b). Further, trees that are closely adjacent to buildings were carefully examined and removed, and the resultant 135 trees were extracted for further analysis (see Figure 3b).
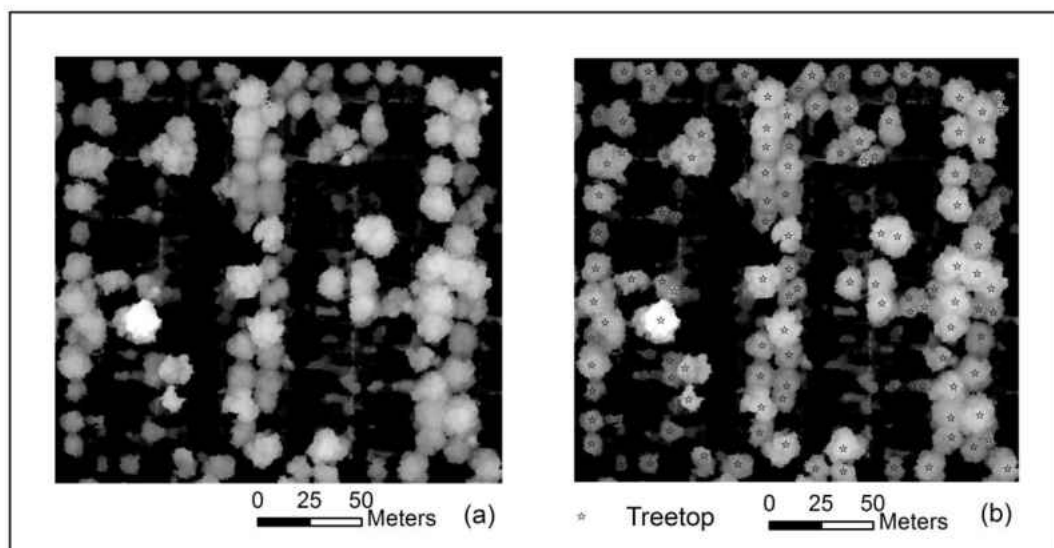
Figure 3 (a) CHM (a) and (b) location of identified trees.

2.4 Methodology

2.4.1   Crown reconstruction

With the location of each treetop, 3D crown surfaces were reconstructed based on a set of generalized geometric models. According to the shapes of crown surfaces, a number of potential models, such as cones, semispheres, half ellipsoids, etc., were employed. Once the models are determined, several essential parameters, including model radius (R), model height (H), and

model curvature coefficient (c), were obtained. The formula of these generalized models is expressed as follows:

$$\frac{((x - x_0)^2 + (y - y_0)^2)^{c/2}}{R^c} + \frac{(z - z_0)^c}{H^c} = 1 \tag{1}$$

where x_0 and y_0 are horizontal coordinates of the treetop; $z_0 = 0$ is the vertical coordinates of the base of a tree identified on the CHM; x and y are the horizontal coordinates of a point on the crown surface; z is the height of the point on the crown surface; R is the radius of model; H is the height of model; and c is the crown curvature coefficient. Among these parameters, R, H, and c are unknown variables.

With a variety of parameters R, H, and c, a number of shapes can be approximated using these generalized models. Especially, a concave shape crown can be obtained with a c value less than 1, a convex shape can be approximated when c is greater than 1, and a cone shape can be created when c is equal to 1. For convex shapes, when R equals to H, a semisphere shape can be obtained with a c value of 2; a shape between cone and semisphere can be obtained with the c value between 1 and 2; and a shape outside of semisphere can be obtained with the c value greater than 2. Further, when R is not equal to H, a number of crown shape scenarios (e.g. cone, half ellipsoid, etc.) can also be obtained (see Table 1 and Figure 4).

Table 1 Model shapes with different parameters

c value	R=H	R≠H
c<1	Concave shape	Concave shape
c=1	Cone	Cone
1<c<2	Between cone and semi-sphere	Between cone and half- ellipsoid
c=2	Semi-sphere	Half-ellipsoid
c>2	Outside of semi-sphere	Outside of half-ellipsoid
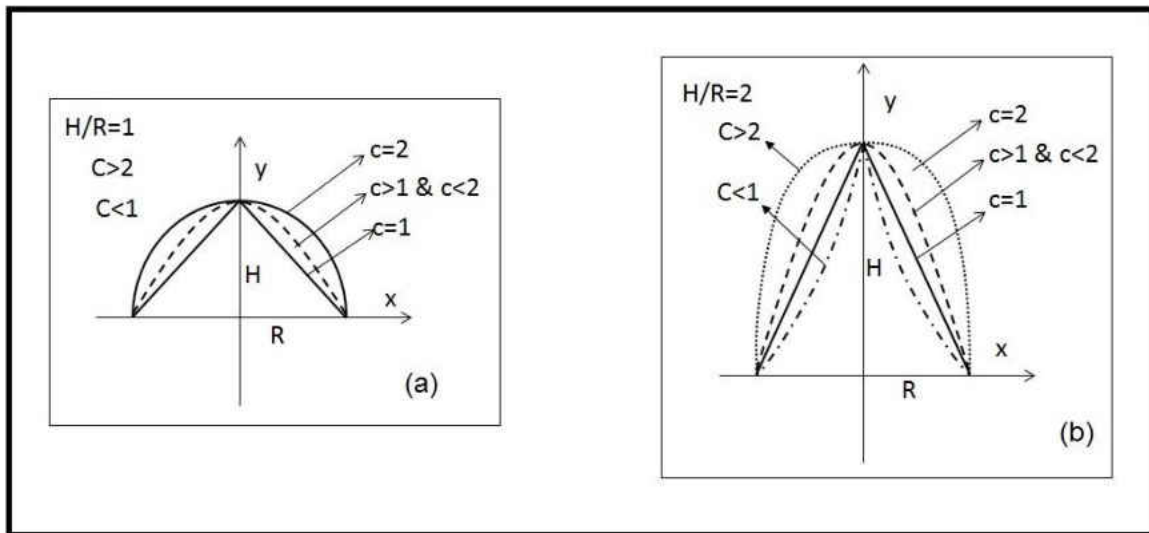
Figure 4 Schematic diagram of crown models.

For each tree crown, model parameters were determined by optimally matching the crown surfaces with available crown shape models. In particular, using the treetops as the centers of circles, the morphological changes of tree crowns were examined, and the radii of circles were determined using sharp slopes (45°) in 8 cardinal directions. Model variables were calculated by using the least squares surface matching (LSSM) approach, which attempts to minimize the

squares of the height difference (SHD) between the modeled surface and LiDAR-derived CHM.

For a given c, the general model equation can be simplified as equation 2 and variables can be

resolved following the equations 3-5.

$$\text{d}^c * X + z^c * Y = 1 \tag{2}$$

Where:

$$\text{d} = ((x - x_0)^2 + (y - y_0)^2)^{1/2}$$

$$X = \frac{1}{R^c}$$

$$Y = \frac{1}{H^c}$$

X, Y can be calculated using the following equations.

$$\begin{bmatrix} d_1^c & z_1^c \\ \vdots & \vdots \\ d_n^c & z_n^c \end{bmatrix} * \begin{bmatrix} X \\ Y \end{bmatrix} = \begin{bmatrix} 1 \\ 1 \\ 1 \end{bmatrix} \tag{3}$$

$$\begin{bmatrix} d_1^c & z_1^c \\ \vdots & \vdots \\ d_n^c & z_n^c \end{bmatrix}' * \begin{bmatrix} d_1^c & z_1^c \\ \vdots & \vdots \\ d_n^c & z_n^c \end{bmatrix} * \begin{bmatrix} X \\ Y \end{bmatrix} = \begin{bmatrix} d_1^c & z_1^c \\ \vdots & \vdots \\ d_n^c & z_n^c \end{bmatrix}' \tag{4}$$

$$\begin{bmatrix} X \\ Y \end{bmatrix} = \left(\begin{bmatrix} d_1^c & z_1^c \\ \vdots & \vdots \\ d_n^c & z_n^c \end{bmatrix}' * \begin{bmatrix} d_1^c & z_1^c \\ \vdots & \vdots \\ d_n^c & z_n^c \end{bmatrix} \right)^{-1} * \begin{bmatrix} d_1^c & z_1^c \\ \vdots & \vdots \\ d_n^c & z_n^c \end{bmatrix}' \tag{5}$$

When X and Y were computed, the heights and radii of crown models with a given c value were determined and the sum of squares of the height difference between the modeled and crown surface were calculated. With a user-defined range of c for all trees, the minimum squares of difference can be acquired through applying an iterative computation process. In this study, the value of c varies from 0 to 3 with an interval of 0.1.

2.4.2 Regression analysis

With the tree crown shape variables derived from the crown re-construction step, we developed regression analysis models to examine the relationship between crown width and these variables. Especially, crown shape variables include LiDAR derived tree height (h), curvature of 3D model (H/R), and crown curvature coefficient (c). In order to analyze the contribution of each parameter in estimating the crown width, 3 regression models with different independent variables were developed. For all these models, the dependent variable was the field measured crown width. Model 1 has only one independent variable: LiDAR-derived tree height (h); Model 2 has 2 independent variables: LiDAR-derived tree height (h) and curvature (H/R) ; and Model 3 includes all 3 crown shape variables: LiDAR-derived tree height (h), curvature (H/R), and the curvature coefficient (c) in the 3D model.

2.5 Results and discussion

2.5.1 Crown reconstruction

Through applying the optimally fitting algorithm, we created 135 geometric models, centered at the treetop locations on the ground (see Table 2 and Figure 5). Each tree has been modeled, using a different shape, and their curvatures range from 0.35 to 9.76, with smaller curvatures

representing lower canopy heights, and larger curvatures indicating higher canopy heights relative to their radii. For example, 9 models have curvatures less than 1, indicating their heights are smaller than their radii. According to the curvature coefficients (see Table 2), we found that 10 models are with cone shapes, 6 models are with half ellipsoid shapes, 38 models are with the shapes between cone and half ellipsoid, and 81 of them are outside of the half ellipsoid shape. Further, we also calculated the average square of height difference (SHD) between a model and the smoothed CHM, which indicates the accuracy of the model in fitting the canopy surface. In this case, the average SHD value is 2.24 m, with 60 of them having SHDs less than 1 meter.

Table 2 Geometric models summary

Curvature (H/R)		Coefficient (c)		SHD	
range	number	range	number	range (m)	number
<1	9	1	10	0-1	60
1-2	42	1-2	38	1-2	20
2-3	48	2	6	2-3	21
3-4	21	2-3	70	3-4	13
4-5	7	3	11	4-5	9
>5	8			>5	12

Note: SHD, the squares of the height difference
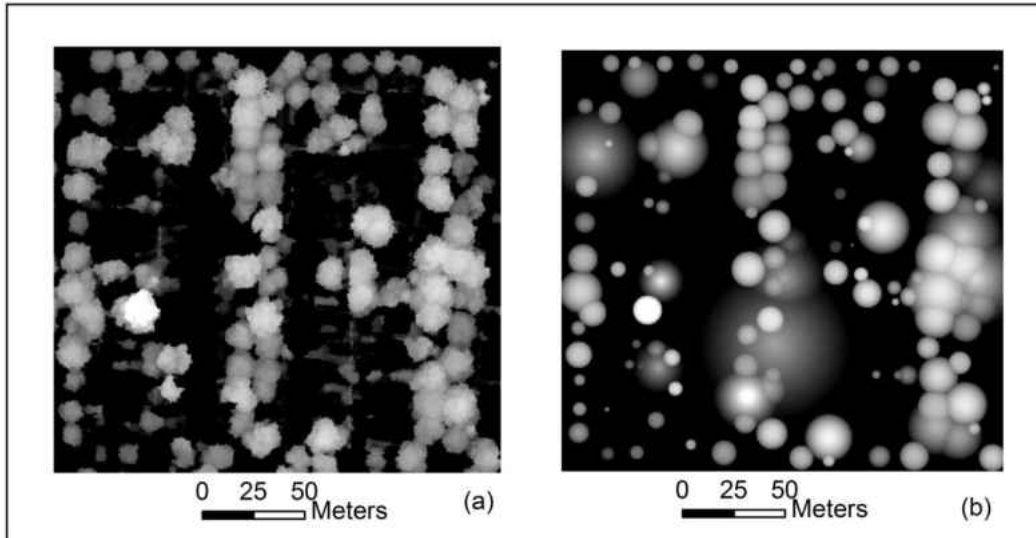
Figure 5 Comparison between (a) tree image and (b) geometric models.

2.5.2   Regression analysis

Through applying the regression analysis methods detailed in Section 4.2, we found that Model 1 explained 54.5% of the variances associated with crown width for all 135 trees, which was significant, $F (1, 133) = 159.14$, mean square of residual ($MS_{residual}$) = 1.55, $p < 0.001$. The mean absolute error (MAE) of the estimates was 0.97 m (17.60 % of dependent mean) and root mean squared error (RMSE) was 1.24 m (22.50% of dependent mean) for 135 trees. The result is consistent with previous studies which reported the tree height can be used for crown width estimation but the accuracy is relatively low. The differences of the species in the study site appear to contribute to the low predictability. Because deciduous trees with large crowns dominate the study area, parameters obtained from Model 1 were mainly determined to represent deciduous trees rather than conifers. Therefore, the predicted crown widths of conifers are much larger than observed ones, and the residual is relatively large (Figure 6a and 6b).

In Models 2 and 3, the shape related parameters were employed for crown width estimation, and results indicate that these 2 models provide better predictabilities when compared to Model 1, but Model 3 slightly outperformed Model 2. The better performances of these two models indicate the importance of tree shape-related parameters in estimating crown width. In particular, the curvature (H/R) represents an essential shape parameter that represents the basic relationship between tree height and crown width. With the addition of the curvature parameters, Models 2 produced higher R^2 of 0.811, a value that was highly significant, $F(2, 132) = 283.26$, $MS_{residual} = 0.65$, $p<0.001$. The MAE decreased to 0.59 m (10.7 % of dependent mean) and RMSE decreased to 0.8m (14.52% of dependent mean) for 135 trees. Moreover, curvature coefficient (c) in the 3D model records the degree of convex or concave of the crown model. With the addition of these 2 shape-related parameters, Model 3 shows a rather intuitive and accurate behavior in crown width estimation for conifers and deciduous trees without obvious outliers (Figure 6e). The value of R^2 for Model 3 was 0.885, which was highly significant, $F(3, 131) = 335.74$, $MS_{residual} = 0.40$, $p<0.001$. The MAE and RMSE further decreased to 0.44 m (8.6 % of dependent mean) and 0.62 m (11.25 % of dependent mean) for 135 trees, respectively.
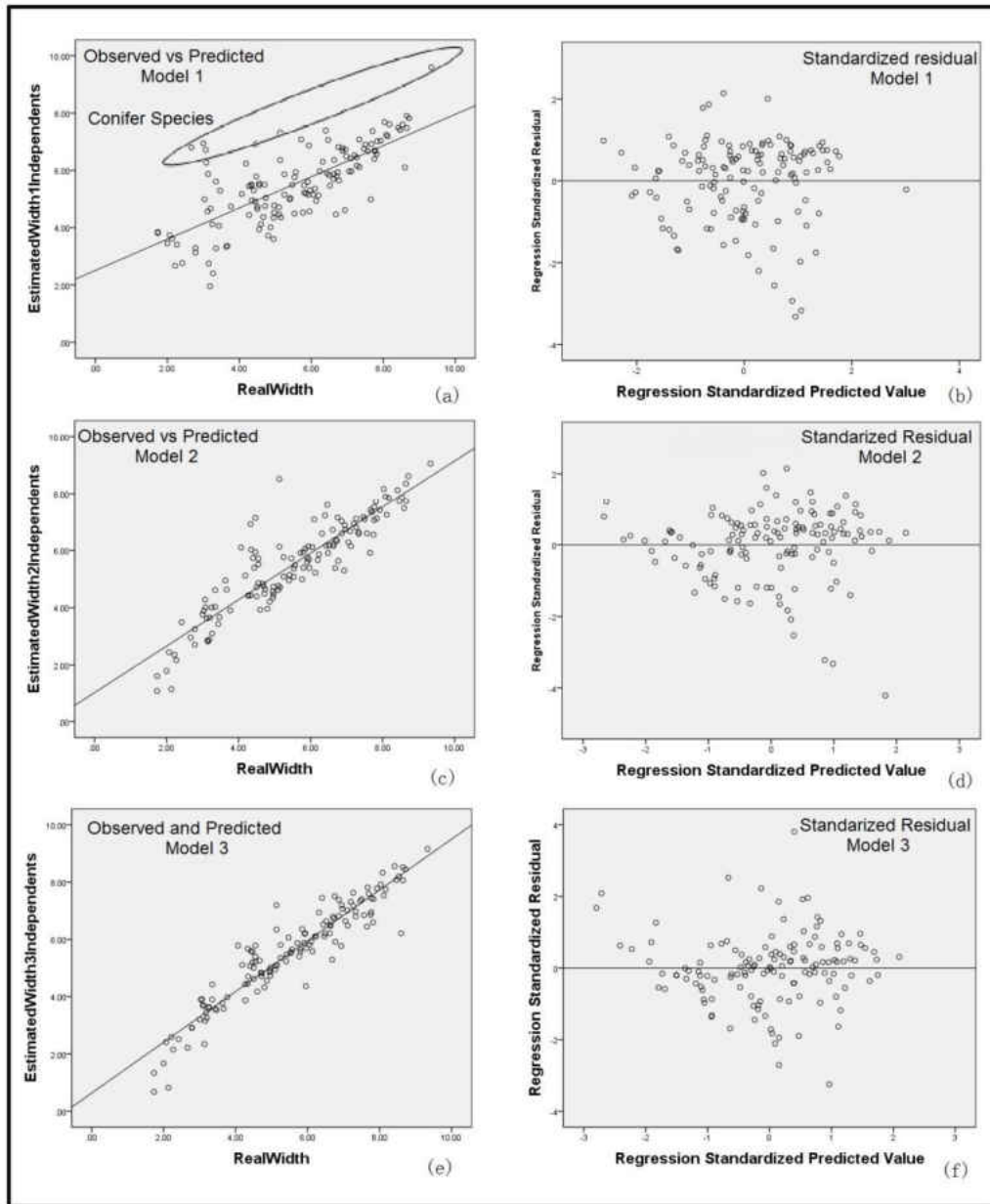
Figure 6 Scatterplots of predicted versus observed crown width and standardized residual.

After the construction of geometric models and accurate estimation of crown width with Model 3, the crown bases can be computed from the geometric models. Through visually comparing the crown model with LiDAR-derived raster image, we can find the boundaries of

each tree model well match the corresponding tree edges (Figure 7). Therefore, the forest canopy can be well segmented based on tree locations and their crown widths.

The regression Model 3 has the ability to accurately estimate the crown width in a mixed forest, but the model relied on not only the shape-related parameters but also the ground measured crown width. The field work would limit the application of this LiDAR processing algorithm in determining a good regression model for estimating crown width using LiDAR
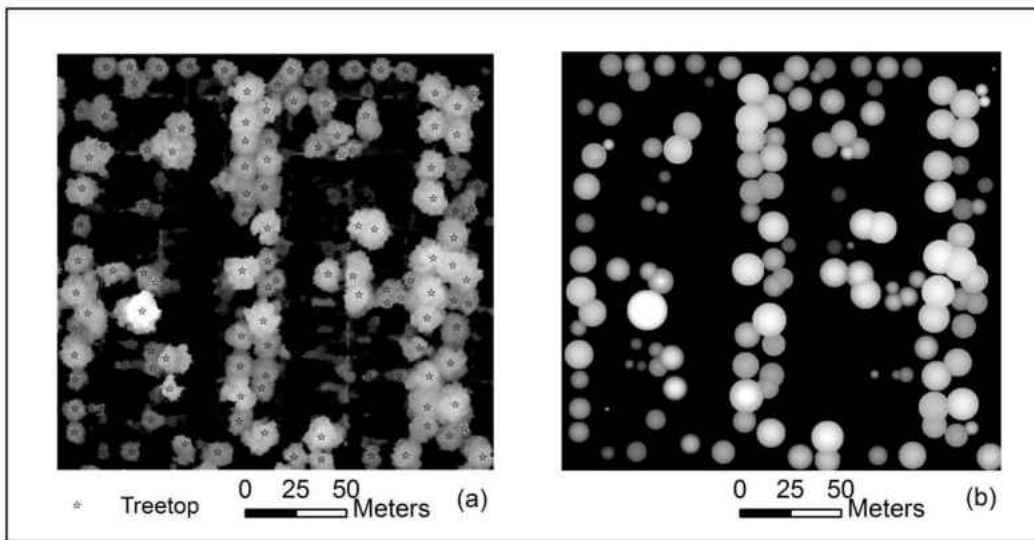
Figure 7 Comparison between (a) tree image and (b) intercepted geometric models.

Table 3 Linear regression results

Model	R^2	MAE (m)	RMSE (m)	Model and significant variable (135 trees)
1	0.545	0.97	1.24	Crown width=0.120+0.397*h
2	0.808	0.59	0.8	Crown width=2.486 + 0.376*h - 1.035*H/R
3	0.885	0.44	0.62	Crown width=-0.563+0.365*h - 1.305*H/R + 2.111*c

MAE: the mean absolute; RMSE: the root mean square error

2.6 Conclusions

Automatic extraction of tree parameters in a mixed forest remains a challenging problem to forest management. Tree boundaries on aerial photos are often blurred, and the process using only tree height to predict crown width neglects species differences. This research illustrates that LiDAR data as a valid source for rapid reconstruction of tree crowns and accurate estimation of crown width in a mixed forest. In addition, data preprocess steps, such as the raw LiDAR points filtering and treetop detection, are necessary to improve the accuracy of geometric model in fitting the crown surfaces. Analyses of results suggest 2 major conclusions.

First, generalized geometric model has the ability to simulate different crown shapes, such as, cones, semispheres, half ellipsoids, as well as other shapes. Centered on treetop locations on the ground, the geometric model of each tree can be created by optimally fitting the LiDAR-derived CHM, using LSSM method. Based on the models, the shape-related parameters such as curvature and curvature coefficient can be extracted for further crown width estimation. However, the geometric model is limited to symmetrical crown and the irregular crown shape has negatively impacted on parameters extraction.

Second, crown shapes are important characteristics of trees, as different shapes correspond to different tree species and the dimension of a tree crown such as ratio between tree height and crown size remains invariant to life stage (Alonzo et al., 2014). Results of regression analysis models indicate that both crown shapes and tree heights contribute to the crown width estimation. The regression model that employed tree height, crown curvature, and curvature coefficient as independent variables has significantly better predictability when compared to other simpler models.

Last but not least, the best model was identified by analyzing all of the trees detected by LiDAR in the study area and the crown widths of many different species, such as Ash, Maple, Oak, Honeylocust, Pine, and Ginkgo trees, have been accurately estimated. Thus, the model and the algorithm may be applied to forests of similar composition and a satisfactory accuracy without any ground measurement can be expected (Table 3).

CHAPTER 3 CROWN-LEVEL TREE SPECIES CLASSIFICATION FROM AISA HYPERSPECTRAL IMAGERY USING AN INNOVATIVE PIXEL-WEIGHTING ALGORITHM

3.1 Introduction

Urban forests play an important role in urban ecological environments in many means, including moderating local climate (Deng et al., 2011), improving air quality (Nguyen et al., 2015), reducing storm-water runoff (Armson et al., 2013), and ameliorating urban heat island effect (Armson et al., 2012). The contribution of urban forests, however, depends on tree species and their spatial distributions (Alonzo et al., 2014). As an example, walnut and poplar have high capacity for carbon dioxide (CO_2) sequestration (Proietti et al., 2016), while holm oak is with the high potential for particle matter (PM) removal thanks to its evergreen nature (Blanusa et al., 2015). Further, sugar maple is one of America's best-loved tree species due to its delicious syrup, value as lumber, and amazing fall color (Whitney and Upmeyer, 2004). Ash trees are widely planted in North American countries due to their high tolerance to surrounding environments (MacFarlane and Meyer, 2005). As the diversity of tree species is a key component for urban forest management (Conway and Vander Vecht, 2015), accurate species mapping is critical for biological diversity investigation (Carlson et al., 2007), effective forest management (Banskota et al., 2011; Plourde et al., 2007), and physiological stress monitoring (Wu et al., 2008).

For mapping tree species, hyperspectral data is considered effective as it can measure subtle variability in spectral reflectance from leaf to crown scales, largely due to their very high spectral resolution and wide range of electromagnetic spectrum. As a result, hyperspectral data have been

widely applied in mapping tree species in urban forests (Alonzo et al., 2013; Green et al., 1998), temperate forests (Heinzel and Koch, 2012), tropical rainforests (Clark et al., 2005), and mountainous forests (George et al., 2014). Species classification has been often carried out at leaf, pixel, sub-pixel, and crown levels. In particular, leaf-level classification emphasizes on differentiating tree species based on the variations of spectral reflectance of leaf samples. Shang and Chisholm (2014) successfully classified seven eucalyptus species in Australia with the best classification accuracy of 94.7%. Clark et al. (2005) achieved 100% leaf-level classification accuracy in discriminating seven emergent tree species in a tropical forest by using linear discrimination analysis (LDA). The relatively pure leaf-level spectra can produce accurate classification accuracy by maximizing between-species spectral variability and minimizing within-species variability. Leaf-level tree species classifications, however, cannot be applied to a large geographic scale as they are labor intensive and time consuming.

In addition to leaf-level techniques, pixel-level classifications have also been employed for tree species classification due to its easiness for implementation and interpretation. Clark and Roberts (2012) classified seven tropical rainforest tree species in Costa Rica from HYperspectral Digital Imagery collection Experiment (HYDICE) data using random forest classifiers. George et al. (2014) classified six broadleaved evergreen and conifer forest tree species in western Himalaya using space-borne earth observation-1 (EO-1) Hyperion dataset. Jones et al. (2010) mapped eleven tree species in the coastal Pacific Northwest, Canada through applying a pixel-level fusion of hyperspectral imagery, a LiDAR derived canopy height model, and a canopy volumetric profile. Dalponte et al. (2012) improved tree species classification in the Southern Alps through integrating LiDAR derived height distribution information and hyperspectral imagery at the pixel level.

Although with some success, pixel-level classification ignores the negative impact of the mixed pixel problem (Lu and Weng, 2004), which may lead to the "salt and pepper" effect in the final classification result (Yu et al., 2006). Subpixel-level classification approaches, therefore, improve tree species classification than traditional per-pixel approaches in dealing with mixed pixels (Huguenin et al., 1997). Subpixel-level classification extracts the proportion of individual land covers of interest within a pixel and results in a more discriminated classification. Bai et al. (2012) employed a linear spectral unmixing approach for forest cover estimation and obtained better results than conventional spectral angle mapper (SAM). Somers et al. (2009) presented a nonlinear spectral mixture analysis (NSMA) for tree cover estimates in orchards. Roberts et al. (1998) developed multiple endmember spectral mixture analysis (MESMA) to map California chaparral in the Santa Monica Mountains. Further, Somers et al. (2010) applied a weighted multiple endmember Spectral Mixture Analysis (wMESMA) to monitor the level of defoliation of Eucalyptus, and achieved improved results when compared to the simple SMA.

Besides leaf level, pixel level, and subpixel level classifications, crown-level classification is increasingly demanded for providing a quantitative estimation of tree species (Dalponte et al., 2013). Several methods have been developed for crown-level species classification. Clark et al. (2005) linearly averaged the pixel spectra within a manually-delineated crown area as the crown-scale spectra for tropical rain forest species classification, and the highest crown-scale classification accuracy of seven species reached 92% with the linear discriminant analysis (LDA) and 30 optimal bands. Zhang and Qiu (2012) developed a treetop-based approach for classifying 40 species classification in an urban forest. Rather than extracting all the pixels within a crown, the treetop-based method identified the single highest pixel per crown for crown-scale spectra extraction, which resulting in an overall accuracy of 69%. Similarly, Dalponte et al. (2013)

conducted a pixel-majority approach for classifying four species in a boreal forest. With this approach, each individual tree crown was assigned to a class if the majority of the pixels with that crown were assigned to that particular class. Further, Alonzo et al. (2013) classified 15 urban forest species with only pixels with normalized different vegetation index (NDVI) values higher than a threshold, and reached an overall accuracy of 86%. Alonzo et al. (2014) integrated Hyperspectral imagery with LiDAR data for mapping 29 tree species in Santa Barbara, California, USA, and an overall accuracy of 83.4% was reported.

Although numerous algorithms, including average pixel method, treetop method, and pixel-majority method (Clark et al., 2005; Dalponte et al., 2013; Zhang and Qiu, 2012), have been proposed for crown-level tree species classification, their accuracies were much lower than those with leaf-level classifications. Leaf spectra, which are often obtained at the laboratory condition, are relatively pure and have proven effective in discriminating tree species (Shang and Chisholm, 2014). Crown-scale spectra, however, have lower purity due to the interference of tree shadows, gaps, trunks, branches, as well as underlying objects (Clark et al., 2005; Shang and Chisholm, 2014; Zhang and Qiu, 2012). This lower purity of crown spectra, therefore, may contribute to the lower classification of tree species at the crown level. In order to address this issue, we developed an innovative method to extract relatively pure crown-scale leaf spectra, which may potentially improve tree species classification accuracy. Specific aims of this paper are: 1) to segment individual crowns using LiDAR derived canopy height model, 2) to calculate the weighted crown-scale spectra from AISA hyperspectral imagery using illuminated-leaf fraction at each pixel as a weighting factor, 3) to classify tree species by applying SVM classifier to the new generated crown-scale spectra. In order to assess the improvement of the pixel-weighting

approach in classifying tree species, the treetop-based and pixel-majority approaches will be carried out for a comparative analysis.

3.2 Study area and data

3.2.1 Study area

The study area is located to the southeast of the University of Wisconsin-Milwaukee (43.07N, 87.87W), located in the Milwaukee City, Wisconsin, United States (see Figure 8). The study site has a geographical area of 300 m*700 m, covering 5 street blocks. The ground surface is flat without significant fluctuation and the average elevation is about 200 m above sea level. This area is dominated by Ash (*Fraxinus* spp.), Maples (*Acer* spp.), Oak (*Quercus* spp.), and some other scattered species, such as Honeylocust (*Gleditsia* spp.) and Pine (*Pinus* spp.). In specific, ash trees are susceptible to the exotic beetle: emerald ash borer (*Agrilus planipennis*, EAB), which have killed tens of millions of native ash trees in the North America (McKenney et al., 2012). The heights of trees along the roads are approximately 5 to 25 m.

Figure 8 (a) Study area in Milwaukee city and (b) true color image.

3.2.2   Dataset

Both AISA hyperspectral imagery and LiDAR data were simultaneously collected by Terra

Remote Sensing Inc. (TRSI) in August 2008. Further, SRA International, Inc. (SRA) and Native

Communities Development Corporation Imaging (NCDC) conducted initial data processing for

AISA hyperspectral and LiDAR data respectively. For AISA imagery, geo-rectification and

radiometric calibration were also performed. As a result, AISA imagery has 366 bands ranging

from 409.85nm to 2,494.57nm, with bandwidth intervals of 4.6 nm in the visible and infrared

(NIR) wavelength, and 6.26 nm in the short-wave infrared (SWIR) bands. The spatial resolution

of these images is 1.0 meter. These images were re-projected to the Universal Transverse

Mercator (UTM) coordinate system (Zone 16N) with a datum of North American Datum of 1983

(NAD83). The LiDAR data were provided in an commonly used binary LASer (LAS) lidar

format with the State Plane coordinate system of Wisconsin South (FIPS 4803) and North

American Datum of 1927 (NAD27). The average point density is 4-5 points/m^2. In addition to

LiDAR and hyperspectral imagery, field data were obtained in September 2015. A total of 198

field trees were identified with the hyperspectral data and four classes were distinguished,

including 1) ash, 2) maple, 3) oak, and other species.

3.2.3   Data preprocess

With the raw LiDAR derived raster images, a large number of randomly distributed dark

holes are visible. This is also called the pit phenomenon, which is caused by the penetration

properties of LiDAR data and the overlaying LiDAR points with different incidence angles from

adjacent flight lines (Ben-Arie et al., 2009; Popescu and Wynne, 2004). In order to remove the

holes under the crown surface and create a smooth canopy height model (CHM), the treetop

height difference (THD) method developed by Liu and Dong (2014) was applied in this research.

Following the THD method, the highest 30 percent of points in the circle filter window with a radius of 1 m were selected to generate a smooth object height model (OHM) (see Figure 9). The smoothed image has a better representation of the crown shape.
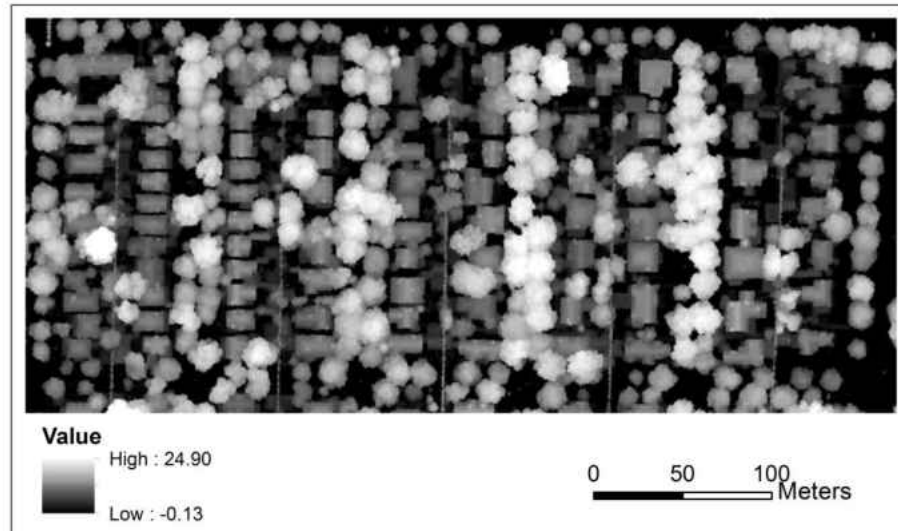
Figure 9 Object Height Model (OHM) derived from filtered LiDAR points.

With the airborne AISA hyperspectral imagery, we performed atmospheric correction using the Quick Atmospheric Correction model in ENVI (Research system, Inc., Boulder, CO, USA). For further processing, water absorption bands (e.g. within the spectral regions of 1335.66-1454.68 nm (bands181-200) and 1786.7-1955.84(bands 253-280)) and the noisy bands (2463.25-2494.57(bands 361-366)) were removed. With remaining 312 bands, we generated a mosaic image (with 1.0 m spatial resolution) and registered it to the gridded LiDAR data (0.2 m). A total of 60 ground control points, such as corners of building and intersections of roads, were selected from the LiDAR derived OHM to geometrically reference the mosaicked AISA imagery, with a root mean square error (RMSE) of 0.2 pixels.

To reduce the interference of non-vegetation for individual tree isolation, the Normalized Difference Vegetation Index (NDVI) was applied to mask out non-vegetation features. As the NDVI values in temperate forests were estimated to range from 0.4 to 0.9 (Cristiano et al., 2014), we adopted the lowest value (0.4) as the threshold to separate trees (NDVI $\geq$ 0.4) from other features (NDVI < 0.4). We derived an NDVI image from the hyperspectral imagery and spatially overlaid with the OHM. The pixels with NDVI values less than 0.4 were assumed as non-vegetation and therefore the corresponding values on the OHM were set as no value. Through applying the NDVI criterion method, other features including roads and buildings were removed from the OHM and the CHM was created to map tree height (see Figure 10).
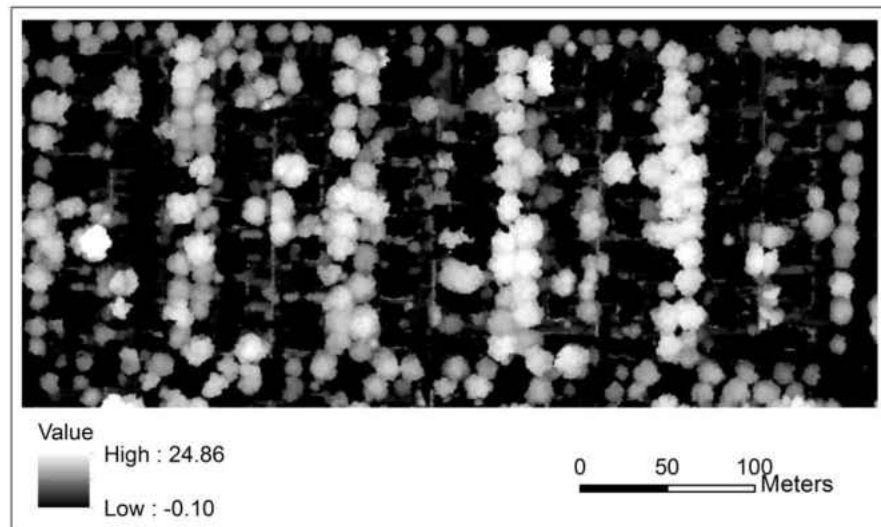
Figure 10 Canopy height model (CHM) map of tree heights.

3.3 Methodology

In this research, three steps have been applied to automatically classify tree species at the crown level, including 1) individual tree crown detection, 2) crown-scale spectra calculation, and 3) tree species classification. These steps are described as follows.

3.3.1 Individual tree crown detection

Individual tree crown detection was achieved with two major steps: treetop identification and crown delineation. Based on the assumption that the highest point in a spatial neighborhood represent the tip of a tree crown (Popescu, 2007), treetops were first identified from the smoothed CHM (Figure 10) using the local maxima (LM) technique with a circular window. The circular window size was determined using a linear regression model developed by Liu and Wu (2016) for this study area. This method is based on the assumption that there is a positive relationship between the height of the trees and their crown sizes (Popescu and Wynne, 2004). Specifically, if a pixel corresponds to the local maximum of a circular shaped window on the CHM, it is marked as a treetop (Popescu and Wynne, 2004). In the second step, the circles centered on the detected treetops were automatically drawn to represent the circular shape of the tree crown observed from above (Doruska and Burkhart, 1994).The circle boundary was determined by the lowest points, called control points, between adjacent treetops. In order to reduce the spectral interference from the adjacent trees, the shortest distance between the treetop and its control points was defined as the radius to generate the circles for individual crown delineation.

3.3.2 Crown-scale spectra calculation

Crown-scale spectra in this study were defined as a weighted average of pixel spectra within a crown region. Due to the presence of mixed-pixel problems and the influence of double-side illuminations (Zhang and Qiu, 2012), the traditional technique of obtaining the crown-scale spectra (e.g. averaging the pixel spectra) blurs within-crown variations and decreases the species classification accuracy (Clark et al., 2005). Therefore, for a better crown-scale tree species classification, pure crown-scale spectra, with which the interferences of non-photosynthetic

vegetation and shadows are mitigated, may improve the tree species classification accuracy. Although many researchers have made efforts to reduce the contamination of non-vegetation on crown-scale spectra using the NDVI threshold (Alonzo et al., 2014; Alonzo et al., 2013; Xiao et al., 2004), few studies have focused on reducing the mixed-pixel and double-side illumination problems in extracting the crown-scale spectra. To address these issues, we employed two sequential steps, including 1) extraction of illuminated-leaf fraction at each pixel using a spectral mixture analysis (SMA) model, and 2) calculation of crown-scale spectra using the illuminated-leaf fractions as weights.

SMA is an effective method to deal with the mixed-pixel problem at the pixel level. It calculates the fraction of a set of endmember spectra within a mixed pixel based on the assumption that the pixel's spectrum is a linear or nonlinear combination of endmember spectra (Adams et al., 1995). When compared with the nonlinear SMA models, linear SMA models were typically utilized to quantify urban compositions due to intrinsic spectral variations (Wu and Murray, 2003). In this research, the constrained linear Spectral mixture analysis (LSMA) was applied to derive the fractional abundances of illuminated-leaf in each pixel for an individual tree crown:

$$R_i = \sum_{k=1}^{n} (f_k R_{ik}) + \varepsilon_i \tag{7}$$

Where R_i is the reflectance of band i for a pixel; i represents a particular spectral band, ranging from 1 to m; f_k is the proportion of endmember k within the pixel, subject to the conditions of $\sum_{k=1}^{n} f_k = 1$ and $f_k \geq 0$; and k labels a particular endmember, ranging from 1 to n; R_{ik} is the reflectance of band i for endmember k; and ε_i represents the error for band i. In this research, the number of spectral bands m is set as 312, and the number of endmembers n is 4.

To obtain f_k, we applied the least squares error estimation method. Once the endmembers are selected and their spectral signatures are generated, the corresponding fraction f_k can be calculated by minimizing the sum of squared errors:

$$\sum_{i=1}^{m} \varepsilon_i^2 = \sum_{i=1}^{m} (R_i - r_i)^2 \tag{8}$$

Where ε_i is the error for band i, m is the number of spectral bands, R_i is observed reflectance spectra of band i, r_i is the estimated reflectance spectra of band i.

Four classes of endmembers were selected in this study for implementing the SMA model. The study area is mainly covered by trees, grass, buildings, and roads. However, a single tree crown may exhibit two different gray values on the hyperspectral imagery due to the double-illumination problem, thus the trees were further divided into illuminated side and shaded side. Therefore, four endmembers include 1) illuminated-leaf (IL), 2) shaded-leaf (SL), 3) green grass (GG), and 4) imperious surface (IS). These endmembers were identified from hyperspectral imagery combined with high-spatial resolution images in Google Earth maps and field survey. IL was selected from the illuminated side of tree crowns and dense crown centers, while SL was identified from shaded side and depressed area of the studied tree crowns. GG was selected from grass-plots presented in front of the buildings in the study area and IS was extracted from the building roofs and roads.

With the pixel values in an individual tree crown as parameters, the pure crown-scale spectra were calculated using a weighted average method. The illuminated-leaf fraction of each pixel calculated through the linear SMA method was set as the weight for each parameter, and the crown-scale spectra were calculated using the following equation:

$$C_i = \sum_{j=1}^{u} (f_j R_j) \Big/ \sum_{j=1}^{u} f_j \qquad (9)$$

Where C_i is crown-scale reflectance spectra of band i for a tree, f_j is the illuminated-leaf fraction within pixel j, R_j is observed spectral value of pixel j, u is the total number of pixels within the crown.

3.3.3 Tree species classification

With the crown-level pixel-weighted spectra for each crown, a support vector machine (SVM) classification algorithm was applied for classifying individual tree species in ENVI image processing environment. SVM is a supervised, non-parametric, and machine learning method that performs classification based on the statistical learning theory (Fauvel et al., 2008). It constructs an optimal separating hyperplane in a higher dimensional space to separate classes. The hyperplane is the decision surface to maximize the distance to the neighboring data points in the classes (Petropoulos et al., 2012a). Linear hyperplane is only efficient for linearly separable samples, and nonlinear hyperplane derived from a variety of kernel functions, such as polynomial, the radial basis function (RBF), and the sigmoid, can represent more complex shapes.

In this research, an SVM with radial basis function (RBF) kernel was chosen as the RBF kernel only requires a small number of parameters but usually produces satisfactory results. Following the ENVI User's Guide (2008), the gamma parameter in the kernel function was set to 0.0032, equal to the inverse of the spectral band numbers (312) of the hyperspectral imagery; the penalty parameter was set to its maximum value (100), meaning that no misclassification occurs during the training process; the number of pyramid was set to a value of zero, forcing the AISA

hyperspectral imagery to be processed at the full resolution; and the classification probability threshold value was set to zero, forcing all pixels to be classified into one class.

3.3.4   Accuracy assessment and comparative analysis

3.3.4.1 Sample selection and accuracy assessment

The classification scheme, consisted of ash, maple, oak, and others, was chosen based on our familiarity with the study area. The total 198 trees were divided into a training data set (around 20%-25%) and a testing data set following the random sampling strategy (see Table 4).

Table 4 Ground reference data in number of trees used in the classification

Class	Total number of trees	Training samples	Testing samples
Ash	51	12	39
Maple	59	12	47
Oak	70	14	56
Other species	18	5	13

Classification accuracy was assessed based on the computation of the overall accuracy (OA), producer's accuracy (PA), user's accuracy (UA), and the Kappa (Kc) statistic (Petropoulos et al., 2012a).

3.3.4.2 Comparative analysis with the treetop-based and pixel-majority classifications

In order to conduct comparative analyses, both treetop-based and pixel-majority classifications were carried out. With the treetop-based classification, the crown-scale spectrum of an individual tree was extracted from the pixel at treetop location in the crown region, and then an SVM classifier was applied to classify the individual tree to a particular species. For

pixel-majority classification, a pixel-based SVM classifier was implemented to assign a species to each pixel, and then an individual tree was assigned to a class if the majority of the pixels within the tree crown belongs to that particular class. During the process of pixel-level classification, six classes, including ash, maple, oak, other tree species, shaded-leaf class, and imperious surface areas, were chosen, with training sites carefully selected from the region. As a result, 800 randomly-selected training pixels were chosen from the corresponding objects for classes of ash, maple, oak, illuminated-leaf, shaded-leaf, and imperious surface areas, and only 200 training pixels were selected as other species due to the limitation of sample availability.

3.4 Results

3.4.1 Individual tree detection

With the local maximum algorithm, the treetops in the study area were detected based on the smooth CHM. The selected trees are distributed along the roads (see Figure 11).
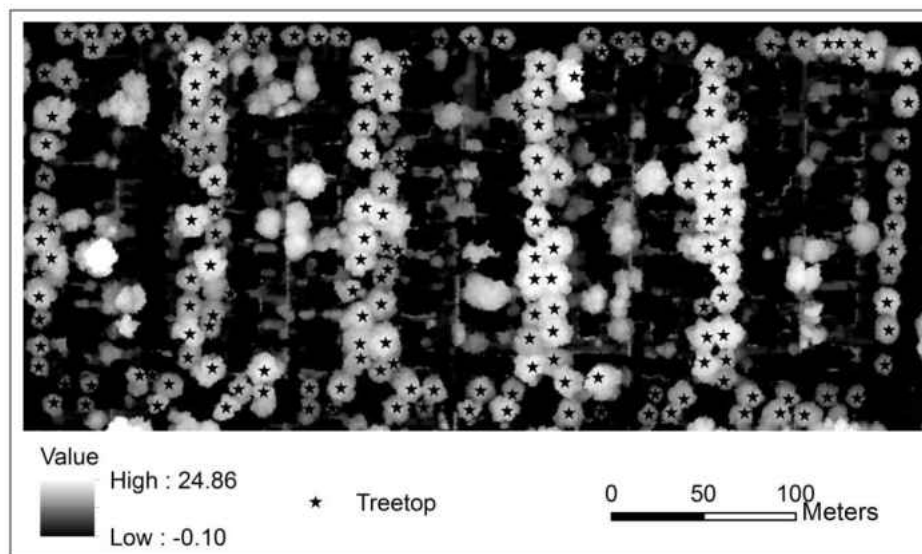
Figure 11 Location of identified trees.

With the shortest distance between the treetop and its control points, the minimum circles centered on treetops were automatically drawn as crown scales (see Figure 12). The average crown radius is 4.32 m, the largest crown radius is 7.28 m, and the smallest crown radius is 2.0 m.
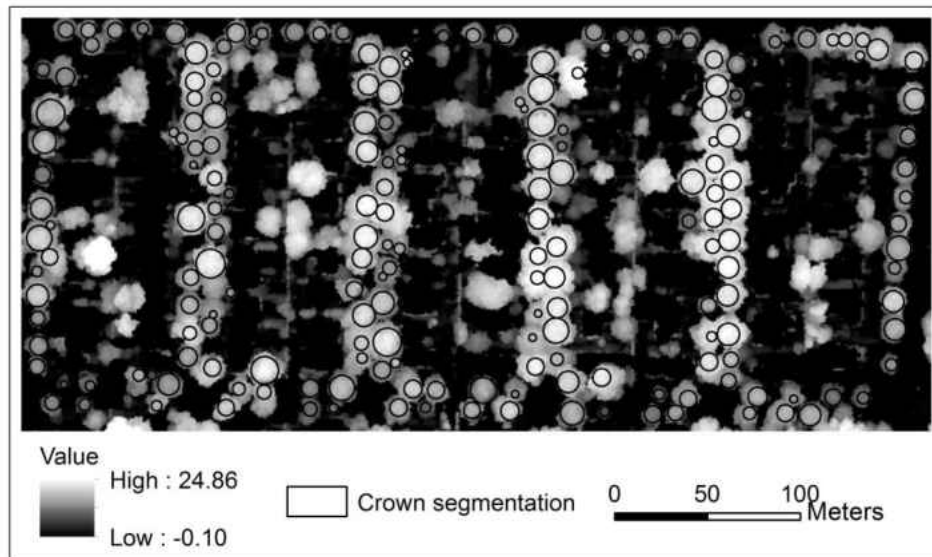
Figure 12 Crown segmentation.

3.4.2   Crown-scale spectra calculation

When the four endmembers of illuminated-leaf, shaded-leaf, green grass, and impervious surface were selected from the hyperspectral imagery, the constrained linear SMA model was applied to quantify their compositions at each pixel and the fraction images were generated (see Figure 13). These fraction images illustrate that the fractions of illuminated-leaves are very high over the sun-side of tree crowns and near 100% in the dense crown center, but crown edges as well as sparse crowns experience low illuminated-leaf fractions (Figure 13a). Besides illuminated-leaf, shaded-leaf fractions also has a clear distribution pattern. The shaded leaves on the canopy not only appear in the back side of the sun but also spread throughout the canopy due

to the roughness of canopy surface (Figure 13b). Moreover, the green grass is observed and covered the open areas along roads, around trees, or in front of houses (figure 13c), and impervious surface areas (e.g. houses) are lined up on both sides of the streets (figure 13d).
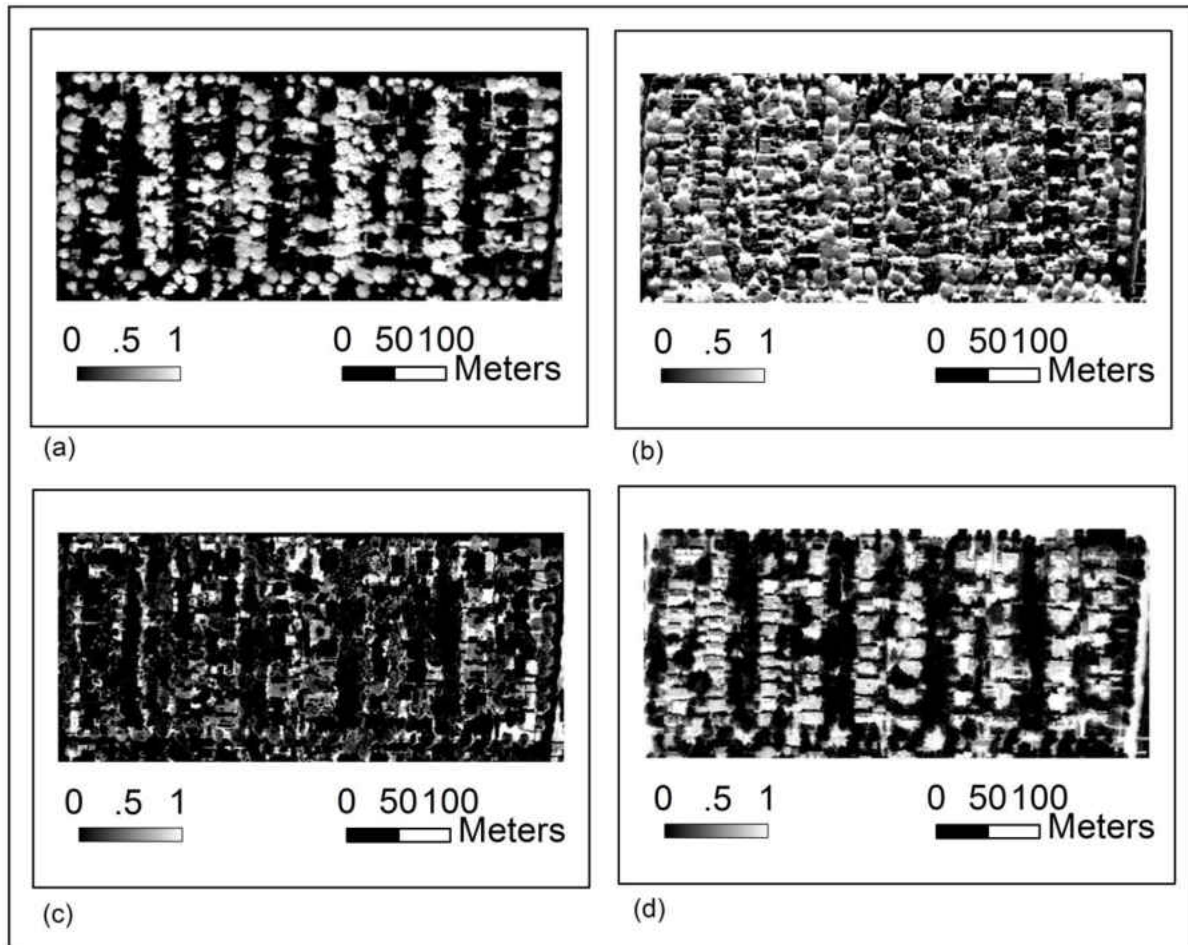
Figure 13 Endmember fractions from linear mixture analysis. (a) illuminated-leaf, (b) shaded-leaf, (c) green grass, (d) impervious surface.

3.4.3   Tree species classification

3.4.3.1 Pixel-weighting classification

Using weighted spectral variables in the SVM classification resulted in an overall accuracy of 80.64% and kappa coefficient of 0.72. Especially, Ash tree species were identified with producer's accuracy of 92.31% and user's accuracy of 80%. Results for Maple and Oak trees were generally better, with the producer's accuracies greater than or equal to 82% and user's accuracy greater than or equal to 75%, but other species have the lowest producer's accuracy (15.38%) but the highest user's accuracy (100%) (see Table 5).

Table 5 Accuracy assessment results of pixel-weighting classification

	Ash	Maple	Oak	Other trees	Total	User's accuracy
Ash	36	2	6	1	45	80.00
Maple	2	39	2	1	44	88.64
Oak	1	6	48	9	64	75.00
Other species	0	0	0	2	2	100.00
Total	39	47	56	13	155	
Producer's accuracy	92.31	82.98	85.71	15.38		
Overall accuracy 80.64%, kappa statistics: 0.72						

3.4.3.2 Treetop-based classification

The classification accuracy with the treetop-based classification approach is significantly lower (e.g. the overall accuracy is 68.38% with kappa statistics of 0.54). The three dominant trees were mapped with producer's accuracies ranging from 61.54% to 80.36% and user's accuracies from 67.16% to 72.73%. In specific, the producer's accuracy of ash tree species is

about 61.54%, and the user's accuracy is approximately 72.73%. Results for other species was also generally lower, with producer's accuracy of 23.08% and user's accuracy of 50% (see Table 6).

Table 6 Accuracy assessment of treetop-based classification

	Ash	Maple	Oak	Other trees	total	User's accuracy
Ash	24	2	4	3	33	72.73
Maple	8	34	5	2	49	69.39
Oak	7	10	45	5	67	67.16
Other species	0	1	2	3	6	50.00
Total	39	47	56	13	155	
Producer's accuracy	61.54	72.34	80.36	23.08		
Overall accuracy 68.38%, kappa statistics: 0.54						

3.4.3.3 Pixel-majority classification

The overall accuracy of pixel-majority classification is 72.26% and the kappa statistics is 0.62, which are much lower than those from the pixel-weighting classification but higher than those from the treetop-based classification. Ash tree and maple have higher user's accuracy (85.71% and 97.14% respectively) but lower producer's accuracy (76.92% and 72.34% respectively). Further, the producer's and user's accuracy of both oak and other species are lower than 70% (see Table 7).

Table 7 Accuracy assessment of pixel-majority classification

	Ash	Maple	Oak	Other trees	total	User's accuracy
Ash	30	2	2	1	35	85.71
Maple	0	34	1	0	35	97.14
Oak	7	8	39	3	59	66.10
Other trees	2	3	14	9	26	34.61
Total	39	47	56	13	155	
Producer's accuracy	76.92	72.34	69.64	69.23		
Overall accuracy 72.26%, Kappa statistics 0.62						

3.5 Discussion

Mapping tree species at the crown-level is essential for urban forests management and physiological stress monitoring (Shang and Chisholm, 2014). As the management unit of practical forest inventories, crown-level tree species could be easily employed to estimate individual tree morality (Yao et al., 2001), analyze forest diversity (Baldeck et al., 2015), and calculate biomass (Mate et al., 2014). As an example, ash tree, one of the most common species in the Milwaukee City, is under the risk of being attacked by EAB (MacFarlane and Meyer, 2005). Accurate identification of ash trees is essential for EAB monitoring and ash tree species protection (San Souci et al., 2009). However, tree species classification using hyperspectral imagery is still a challenge task due to the mixed-pixel problem and double-side illumination problem at the crown level.

Our study has shown that the proposed pixel-weighting classification is an effective approach for separating tree species in the urban area of Milwaukee (e.g. overall accuracy is 80.64%, kappa statistics is 0.72). For the three major species, producer's accuracies are greater than 82% and user's accuracies are greater than 75%. The pure crown-scale spectra extracted from the training and testing samples contributed to higher classification accuracies. For ash trees, in particular, the producer's accuracy reaches 92.31% and the user's accuracy reaches 80%. The other species class has lower producer's accuracy because it contains several species with different reflectance, such as, honeylocust, pine, ginkgo, etc..

The proposed pixel-weighting classification method has the following major advantages when compared with the treetop-based and pixel-majority approaches. First, this method has successfully addressed the mixed-pixel problem and mitigated the adverse effects of tree shadows, gaps, and other non-photosynthetic vegetation on tree species classification. That is, instead of merging or averaging pixels within a crown directly (Dalponte et al., 2012), this method applied a spectral mixture analysis (SMA) and a pixel-weighting approach to extract crown-scale leaf spectra, thereby decreases within-species spectral variability and between-species spectral confusion, and further improves the accuracy of the tree species classification. Second, the pixel-weighting approach is less sensitive to crown delineation error and outliner pixels. The crown-scale spectra were derived through a weighted average of the pixels' spectra, with the illuminated-lead fractions as the weights. Therefore, pixels containing gap or other materials around the crown boundaries have little contribution to crown-scale spectra due to their low weights, while pixels with higher illuminated-leaf fractions have larger contributions. As a result, the pixel-weighting classification is less likely to suffer from outlier pixels and crown delineation errors. Third, the pixel-weighting classification also benefits from the machine

learning algorithm (SVM) in the crown-level tree species classification. SVM can maximize the separation by fitting an optimal separating hyperplane and perform better than other classifiers, such as spectral angle mapper (SAM) and artificial neural network (ANN) (George et al., 2014; Petropoulos et al., 2012a).

3.6 Conclusions and future work

This research developed a pixel-weighting approach for crown-level tree species classification in urban forests. This innovative method combined the constrained LSMA model and weighted average algorithm to extract crown-scale spectra, and applied an SVM classifier to classify tree species at the crown level. The major advantages of this method include: 1) pixel-based illuminated-leaf fraction was extracted using the constrained linear SMA model, which mitigated the mixed-pixel problem at the pixel level; 2) pure crown-level spectra were calculated using a weighted average algorithm, which mitigated the interferences of non-photosynthetic vegetation and shadows; and 3) tree species classification accuracies were improved by applying the SVM classifier. Classification results and comparative analysis suggest that pixel-weighting approach is effective to automatically classify four tree species at the crown level in the Milwaukee City. It produced an overall accuracy of 80% and the kappa statistics of 0.72 for ash, maple, oak, and other species, which were significantly better than those generated with treetop-based and pixel-majority approaches. Ash species, in specific, were successfully identified with higher producer's accuracy (92%) and user's accuracy (80%). The weighted crown-scale spectra reduce the interference from shadow, gaps, and bare earth, and further improve the ash species classification.

Although the results of crown-level tree species are satisfactory, further improvements may include the applications of the multiple endmember spectral mixture analysis (MESMA) for pure

58

crown-scale spectra calculation. MESMA allows the number and the types of endmembers to vary pixel by pixel across an image, thereby overcoming the limitations of linear SMA which using the same endmembers to model all image pixels (Quintano et al., 2013). Thus, MESMA has potential for improving pure spectra extraction. Moreover, individual crown structure features derived from LiDAR data, together with the developed crown-level pixel-weighted spectra, may have potential for further improving tree species discriminations.

Acknowledgements

CHAPTER 4 TREE SPECIES CLASSIFICATION BASED ON THE FUSION OF AISA HYPERSPECTRAL IMAGERY AND DISCRETE LIDAR DATA

4.1 Introduction

Urban trees play a major role in providing ecosystem services (Manes et al., 2012), such as mitigating heat stress, improving air quality, reducing building energy use, stabilizing ozone removal rate, and thereby enhancing human health (Akbari, 2002; Nowak et al., 2006; Pataki et al., 2011). Further, the diversity of tree species reduces the risk of catastrophic loss of trees from pests and diseases in comparison with genetically similar trees which have a similar susceptibility to biotic stress (Kendal et al., 2014). Higher levels of diversity also provide a greater capacity for urban forests to adapt to climate change (Alvey, 2006), including less sensitivity to drought and heat waves (Manes et al., 1997). Additionally, exposure to a diversity of species provides positive psychological and physiological effects (Cilliers, 2010; Goddard et al., 2010). Given the benefits of urban biodiversity, information about the current patterns of tree species composition is needed for supporting management efforts (Conway and Vander Vecht, 2015). Tree species classification based on remote sensing techniques has been widely employed and provided an attractive alternative to field surveys in forest inventory due to its lower total cost, greater geographic coverage, and higher efficiency(Holmgren and Thuresson, 1998; Zhang and Qiu, 2012).

Hyperspectral imagery and LiDAR data are two favorite data sources for tree species classification. Hyperspectral imagery is generally composed of hundreds of relatively narrow but continuous spectral bands from visible to shortwave infrared parts of the electromagnetic spectrum (Petropoulos et al., 2012a). Thus, the vast amount of spectral information provides the

most valuable information for tree species classification and plant disease identification. George et al. (2014) employed the Earth Observation-1 (EQ-1) Hyperion hyperspectral imagery with 242 bands to discriminate six broadleaved evergreen and conifer forest tree species in western Himalaya, and the best overall accuracy was 82.27% and the kappa statistic was 0.79. Xiao et al. (2004) utilized airborne visible/infrared imaging spectrometer (AVIRIS) imagery with 224 bands to map 22 urban tree species in Modesto, CA, which resulted in an average accuracy of 70%. Alonzo et al. (2013) also used AVIRIS imagery to identify 15 common urban tree species, and the overall classification accuracy reached 86%. Zhang and Qiu (2012) employed the airborne imaging spectrometer for application (AISA) hyperspectral images with 492 spectral bands to identify 40 urban species in Dallas, Texas with 69% overall accuracy. Clark et al. (2005) applied the HYperspectral digital imagery collection Experiment (HYDICE) data with 210 bands for the discrimination of seven tropical rainforest tree species. Dalponte et al. (2012) evaluated the potential of two high spectral and spatial resolution hyperspectral imageries (HySpex-VNIR 1600 and HySpex-SWIR 320i) for classifying four tree species in boreal forests. The visible and near infrared (VNIR) hyperspectral bands were found more effective in discriminating boreal species than those bands in the medium infrared (SWIR) range. Although hyperspectral data has performed relatively well in tree species classifications, the similarity of spectral signatures of different tree species and the 2-dimensional (2D) properties of optical remote sensing data still challenge the successful tree species classification (Ghosh et al., 2014; Jones et al., 2010).

In contrast, LiDAR data provides the vertical distribution of vegetation elements above the ground along with the measurement of terrain elevation. LiDAR is particularly suited to derive information relevant to biophysical vegetation properties such as tree height, fraction vegetation cover, canopy geometry, and above-ground biomass (Lefsky et al., 2002; Morsdorf et al., 2006).

Naesset (1997) computed the mean tree height from an airborne laser scanner using the arithmetic mean and the weighted mean of the canopy heights within each stand. Popescu et al. (2003) fitted two perpendicular profiles of a tree crown using a fourth-degree polynomial curve and calculated the crown diameter as the average of these two values along the profiles. Results suggested that approximately 62% of the variances were associated with diameter for dominant trees. Kato et al. (2009) not only measured tree height and crown width but also captured crown base height and crown volume through surface reconstruction using LiDAR data. Popescu (2007) estimated aboveground biomass and biomass components for individual trees using linear and nonlinear regression analyses, and results suggested that LiDAR derived tree height and diameter at breast height (dbh) proved to be particularly important for biomass prediction. Besides the extraction of the geometric and biophysical properties, high density airborne LiDAR data are also suitable for specific tree species classification. Ørka et al. (2009) discriminated 197 Norway spruce and 180 birch trees in Norway using airborne laser scanner (ALS) derived structural and intensity features, which resulted in an overall classification accuracy of 88%. Li et al. (2013) successfully classified four tree species with an overall accuracy of 77.5% based on several LiDAR derived structure features, such as 3D texture, foliage clustering degree, foliage clustering scale, and gap distribution of individual trees. Although LiDAR provides a set of crown structural variables, it alone is not sufficient for species discrimination in a biodiverse forest with large numbers of species (Alonzo et al., 2014).

LiDAR data can describe the geometric properties of vegetation by sampling the spatial dimensions, while hyperspectral imagery measures biotic properties of vegetation by sampling the spectral dimensions (Koetz et al., 2008), thus the synergistic use of LiDAR and hyperspectral data is regarded as a promising technique to enhance comprehensive canopy characterization,

increase the segmentation capability, and improve tree species classification (Hill and Thomson, 2005; Voss and Sugumaran, 2008). Dalponte et al. (2008) directly joined the LiDAR derived height and intensity information with the 40 selected bands of AISA hyperspectral imagery in classifying 23 tree classes and increased the accuracy by more than 5% for 5 classes. Jones et al. (2010) integrated LiDAR-derived CHM and canopy volume profile (CVP) data with hyperspectral imagery at the pixel level in mapping 11 tree species in the Gulf Islands National Park Reserve, Canada, and reported improved producer's (+5.1-11.6%) and user's (+8.4-18.8%) accuracies for dominated species. Dalponte et al. (2012) generated 19 height related bands based on LiDAR features within each pixel (e.g. maximum, minimum, and average of height point within each pixel) and joined 6 optimal bands with hyperspectral imagery for tree species classification at different level. The results indicated the fusion of LiDAR and hyperspectral data increased the classification accuracies at the levels of macro classes, forest types, and forest species. In comparison with fusion at the pixel level, crown-level fusion has more potential for tree species classification due to the improvements of crown segmentation and structural metrics extraction from 3D LiDAR data. Zhang and Qiu (2012) simply integrated LiDAR and hyperspectral data for urban tree species classification. LiDAR data was used for individual tree detection while hyperspectral data was used for species classification. Further, Alonzo et al. (2014) extracted 28 structural metrics directly from 3D LiDAR point cloud and fused them with all spectra exceeding an NDVI threshold of 0.6 within a crown. The addition of LiDAR data increased 4.2% of overall accuracy compared to spectral data alone.

Fusion of hyperspectral imagery and LiDAR data has benefit tree species classification by fully exploiting both spectral and spatial information. A number of researchers have integrated CHM, CVP, and/or LiDAR intensity information with hyperspectral imagery to increase the

pixel-level classification accuracy, and many studies focused on the fusion of hyperspectral imagery and crown attributes, such as crown height and crown width metrics, to improve the crown-level classification. However, these fusions have two disadvantages in tree species classification. First, these biophysical properties are not identical within the same tree species. For example, tree height increases and crown size extends as tree grows, crown volumes may vary with different crown architectures, and LiDAR intensity depends on many variables, such as local incidence angle, path length, transmit pulse energy of laser, etc. Therefore, these features play limited contributions in mixed forests. Second, these fusions ignore the mixed pixel problem in hyperspectral imagery. Shadow, gap, and other materials within a crown may adversely affect the spectral reflectance and decrease the tree species classification. To address these issues, crown shape index (SI) and coefficient of variation (CV), corresponding to height distribution and height dispersion, were extracted from LiDAR data as the invariant features in tree's life cycle, and tree height was extracted as well for comparison purpose. In addition, both treetop-based and pixel-weighted spectra were extracted from hyperspectral imagery. Treetop-based spectrum suffers less mixed-pixel problem and double-illuminated problem due to distance from crown boundary, while pixel-weighting spectra were calculated using illuminated leaf fraction within each pixel as weight factors to measure pure spectra at crown level. Finally, tree height, SI, and CV were fused with treetop-based and pixel weighted spectra respectively for tree species classification. The specific objectives include: 1) identifying individual trees from LiDAR data, 2) extracting structural features from LiDAR derived CHM, 3) extracting spectral features from AISA hyperspectral imagery, and4) fusing spectral and structural features for tree species classification.

4.2 Study area and data

4.2.1 Study area

The study area is located in the Upper East Side neighborhood of Milwaukee, Wisconsin (43.07N, 87.87W), covering a 300 m * 700 m area (see Figure 14). As the largest city in the state of Wisconsin, Milwaukee lies on the western shore of Lake Michigan and the humid continental climate supports a diverse mix of urban forest trees. The study area is dominated by several deciduous trees, such as ash (*Fraxinus* spp.), maples (*Acer* spp.), oak (*Quercus* spp.), honeylocust (*Gleditsia* spp.) and some scattered coniferous trees such as pine (*Pinus* spp.) and spruce (*Picea* spp). The terrain in the study area was sculpted by a glacier path. The average elevation of the relative flat surface is about 200 m above sea level and tree heights are approximately 5 to 25 m.
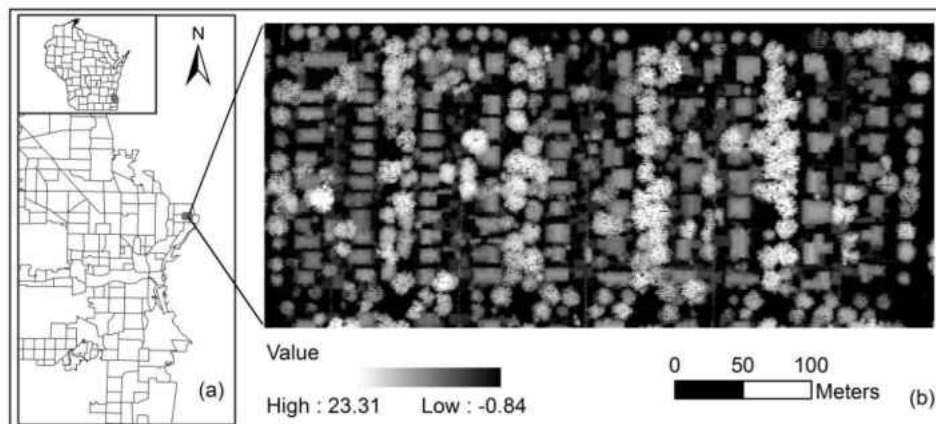

Figure 14 Study area in Milwaukee (a) and canopy height model (b).

4.2.2 Data set

The airborne imaging spectrometer for application (AISA) hyperspectral imagery was acquired by Terra Remote Sensing, Inc. (TRSI) using an AISA hyperspectral sensor in August 2008. The imagery has a spectral range between 409.85 nm and 2494.57 nm and a total of 366

spectral bands. The spectral resolution in the visible and infrared (NIR) wavelength is 4.6 nm and the resolution in the short-wave infrared (SWIR) wavelength is 6.26 nm, while the spatial resolution is 1.0 meter. LiDAR data were collected by TRSI in August 2008 as well, but Native Communities Development Corporation Imaging (NCDC) led the LiDAR data analysis and provided the final LiDAR data with the coordinate system of NAD 1927 State Plane Wisconsin South (FIPS 4803) and mean point density of 4.5 points per m^2. Besides the remote sensing data, field data were collected in September 2015. In total, 198 LiDAR-detected trees along the roads in the study area were identified and grouped into ash, maple, oak, and other species.

4.2.3 Data preprocess

To remove the effects of the atmosphere on the two images spanning the study area, the Quick Atmospheric Correction Model in ENVI (Research system, Inc., Boulder, CO, USA) was first carried out for atmospheric correction. And then the water absorption bands (bands 181-200 and bands 253-280) corresponding to the spectral regions of 1335.66-1454.68 nm and1786.7-1955.84 nm as well as the noisy bands (bands 361-366) corresponding to the spectral region of 2463.25-2494.57 nm were removed. Subsequently, a single image with 1.0 spatial resolution was generated by mosaicing the images covering the whole study area and co-registered to the gridded LiDAR data (0.2 m) based on 60 ground control points and nearest neighbor resampling. The control points were selected from corners of building and intersections of roads, and the root mean square error (RMSE) was 0.2 pixels.

Due to LiDAR characteristics of penetrating through forest canopy, data pits, randomly distributed exceptionally lower height value in a raster, are typically distributed in canopy height model which was interpolated from the raw LiDAR data (Popescu and Wynne, 2004). These pits may adversely affect the crown segmentation, tree height estimation, and forest biomass

calculation (Ben-Arie et al., 2009). Therefore, extraction of LiDAR points on the crown surface rather than within the crown is prerequisite to create a smooth crown surface. In this research, we applied the treetop height difference (THD) method (Liu and Dong, 2014) to selected the highest 30 percent points of search windows with a radius of 1 m and interpolated them into the smooth canopy height model (CHM) (see Figure 15).
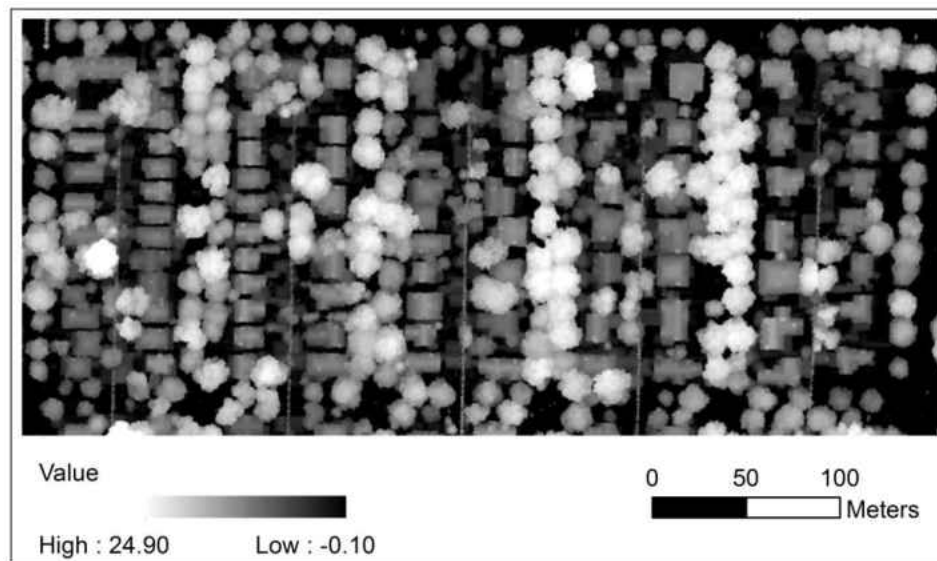
Figure 15 Smooth canopy height model (CHM).

4.3 Methodology

To automatically and accurately classify tree species at the crown level, the main steps of the process includes: 1) individual tree identification based on smooth CHM, 2) structural feature extraction from individual tree crowns, 3) crown-scale spectra calculation from hyperspectal imagery, and 4) data fusion for tree species classification. These steps are presented as follows.

4.3.1 Individual tree identification

Individual trees were identified on the smooth CHM in two major steps. The locations of tree tops were first detected with a local maximum (LM) filtering method (Popescu and Wynne, 2004). The LM technique operates on the assumption that the highest point in the spatial neighborhood represents the treetop of a tree crown, and the window size to search for the tree top is dependent on the strong relationship between the tree height and the crown size (Popescu, 2007; Popescu and Wynne, 2004). Specifically, a circular shaped window moves through the CHM, if a given pixel is the highest than all other pixels within a search window, it is identified as a treetop, wherein the window radius was automatically calculated using a linear regression model developed by Liu and Wu (2016). Second, the tree crown delineation operated on the assumption that the lowest points between two crowns are the control points on the boundary to separate them. In response to the circular crown shape observed from above, circles were automatically drawn on CHM as crown scales. The centers of circles were located at treetop location and the circle radii were calculated as the average distance between the treetop and its control points.

4.3.2 Structural feature extraction from LiDAR data

The structure of a tree crown is defined as the distribution of all the plant elements (e.g. leaves, twigs, branches, etc.) and their geometric properties (e.g. size, shape) within the tree crown (Wang and Jarvis, 1990). The structural properties have a significant effect on radiation absorption, photosynthesis, and transpiration, and they can be derived from the discrete LiDAR data. As the most basic and intuitive attribute, tree height plays an important role in forestry and forest ecology (St-Onge et al., 2004), and many other features, such as the biomass and DBH,

were calculated dependent on it (Ørka et al., 2009). Therefore, tree heights, in this research, were chosen as the first structural feature for tree species classification.

Crown shape is another feature suited to distinguish species because it is more invariant to life stages and can capture between-species variability in crown morphology (Alonzo et al., 2014). And the three-dimensional (3D) shape signature was developed by Osada et al. (2002) to measure geometric properties of the 3D object. 3D shape signature describes the probability distribution samples from a shape function and therefore reduce the 3D matching problem to the comparison of 2D probability distribution. In this study, the shape signature measuring the frequency distribution of the heights at random points on a crown surface was carried out, and then the shape index, one-dimensional expression of shape signature in measuring geometric properties of the 3D object, was further calculated for tree species classification. In particular, when the number of random points, such as 5000, was determined, the points within a crown scale were randomly selected and their heights were extracted from the crown surface, and then the values were sorted and put into user defined histogram bins, such as 100, to show the height frequency. Based on the height shape signature, the shape index was calculated using the following equation:

$$SI = \sum_{i=1}^{m} (i * b_i) / \sum_{i=1}^{m} b_i \qquad (10)$$

Where, m is the number of bin, b_i is the value in bin i.

In addition to SI, a third index, coefficient of variation (CV) describing the height dispersion within a crown scale, was proposed. CV is known as relative standard deviation (RSD) measuring the variability of a series of numbers independent of the unit (Abdi, 2007). Comparing

with the absolute variability of standard deviation, CV is a helpful statistic in comparing the degree of variation from one data series to another with considerably different means. Whereas, CV is defined as the ratio of the standard deviation σ to the mean E:

$$CV = \frac{\sigma}{E} \tag{11}$$

Where $E = \frac{1}{n}\sum_{j=1}^{n} X_j$ and $\sigma = \sqrt{\frac{1}{n}\sum_{j=0}^{n}(X_j - E)^2}$; n is the number the samples, X_j is the value of the sample j.

4.3.3 Spectral feature extraction from AISA hyperspectral imagery

Crown-scale spectra were extracted with two methods: treetop-based and pixel-weighting approaches. Treetop-based method directly extracted the spectrum of the pixel at treetop location as the crown spectrum of an individual tree. Treetop pixel, located in the center of a tree crown, suffers less pixel mixture problems caused by gap, shadow, and other species, which usually occur around crown boundaries. In addition, treetop, as the highest point, is rarely impacted by double-sided illumination problems, which are common on two sides of crown scales (e.g. sun-side, shaded-side) (Zhang and Qiu, 2012). Therefore, treetop pixel is the best portion of a tree crown to represent the spectral signature of an individual tree and treetop-based spectra were extracted for tree species classification in this research.

Pixel-weighting method calculated the weighted average of pixels' spectra within tree crowns as crown-scale spectra. In this research, the pixel spectrum was assumed as a linear combination of four endmember spectra, including illuminated-leaf, shaded-leaf, grass, and impervious surface. Therefore, the proportions of the endmembers within each pixel were extracted by a constrained linear spectral mixture analysis model (Wu and Murray, 2003), and

the illuminated-leaf fraction was defined as the weighted factor for each pixel to calculate the crown-scale spectra. The pixel-weighting method mitigated the mixed-pixel problem and double-side illumination problem. Thus the resulted pixel-weighted spectra have the capacity of measuring the pure crown-scale spectra and classifying tree species with high accuracy.

The redundancy of full hyperspectral datasets is not efficient or reliable due to Hughes' phenomenon, which arises when the ratio between the number of training samples and the number of features is small (Hughes, 1968). Therefore, the optimal spectral subsets are necessary to be selected for maximizing the discrimination of target features (Jones et al., 2010). In this study, a stepwise discriminant analysis based on Wilk's lambda method was carried out using SPSS (ver.22) to reduce the dimensionality of the hyperspectral data. Wilk's Lambda is a multivariate analysis of variance, and it corresponds to the ability of each band to separate the tree classes, the lesser the Wilk's lambda, the greater the separability between the different classes (George et al., 2014). When applied the software on treetop-based and pixel-weighted spectra, the two corresponding sets of optimal bands were selected.

4.3.4 Data fusion and Classification

In order to assess the contribution of different structural features to tree species classification, treetop height (TH), shape index (SI), and coefficient of variation (CV) were integrated with the optimal treetop-based and pixel-weighted spectra respectively. Therefore, the fused datasets were divided into two groups: treetop-based spectra/structural dataset and pixel-weighted spectra/structural dataset. Each group consisted of the following four variables.

1) Optimal hyperspectral bands (Spectral only)

2) Optimal hyperspectral bands + tree height (Spectral + TH)

3) Optimal hyperspectral bands + shape index (Spectral + SI)

4) Optimal hyperspectral bands + coefficient of variation (Spectral + CV)

During the classification process, a non-linear support vector machine (SVM) classifier was applied. SVM has been proven better than conventional approaches in performing classification in complex environments, as it finds the hyperplane to maximize the margin between different classes (Petropoulos et al., 2012). Comparison with the linear hyperplane, kernel functions can represent more complex shapes and operated in high dimensional space. The radial basis function (RBF) kernel SVM was chosen in this research due to better performance and less number of required parameters. Based on ENVI User's Guide (2008), the parameters of gamma γ and penalty C were set as 0.0032 and 100 respectively. γ is the inverse of the number of the spectral bands and C controls the cost of misclassification on the training data. The number of pyramid and the classification probability threshold were set as zero to force the imagery processed at full resolution and each pixel was classified into a class.

4.4 Results and discussion

4.4.1   Individual tree identification

Treetops in the study area were first detected using the local maximum method on the LiDAR-derived canopy height model. Due to the inaccessibility of trees in private properties for field survey, only trees along the roads were selected for species classification accuracy analysis. With the average distance between the treetop and its control points as the radius, the circles centered on treetops were automatically drawn as crown scales. The identified treetop and crown scales can be seen in Figure 16.
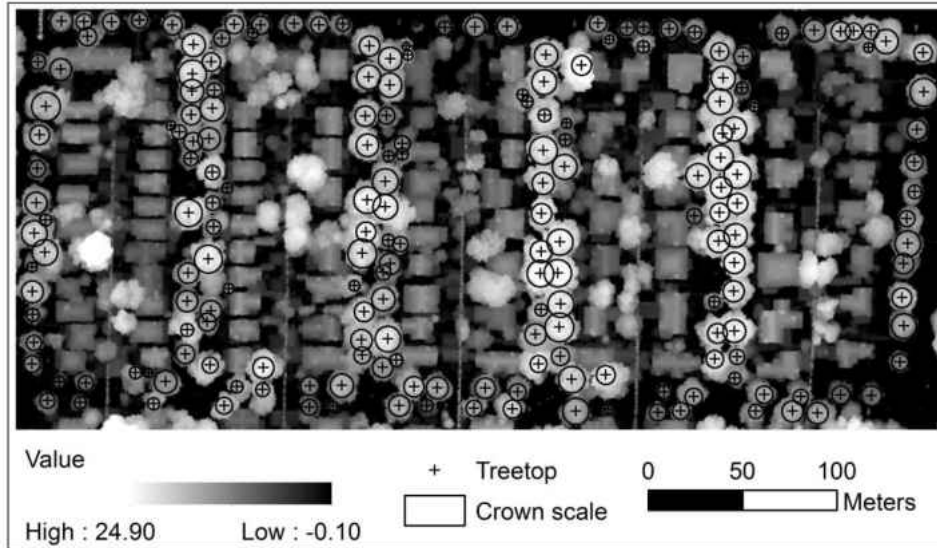
Figure 16 Treetops and crown scales.

4.4.2   Structural feature extraction from LiDAR data

Based on the smooth CHM and crown segmentation, three structural features including tree
height, crown shape index (SI), and coefficient of variation (CV) were extracted (see Figure 17).
First, tree heights were obtained by directly measuring the pixel values at the treetop locations.
The tallest tree reaches 20.62 m and the shortest one is only 5.97 m, the average height at 14.04
m (see Figure 17a). Tree heights are mainly located and distributed between 10 m to 20 m.
Second, shape indices were computed and varied in the range between 52.16 and 92.87, with an
average value of 82.02 (see Figure 17b). The low value indicates the crown has a steep slope,
while the high value represents the crown has a relatively flat surface. The large number of shape
indices with high values is consistent with the dominance of the deciduous tree species in the
study site. Third, coefficients of variation were calculated by dividing the standard deviation by
the mean (see Figure 17c). They are distributed between 2.15% and 21.4% with an average of
7.87%. The low value in our study indicate low variability of the heights within a crown.

73
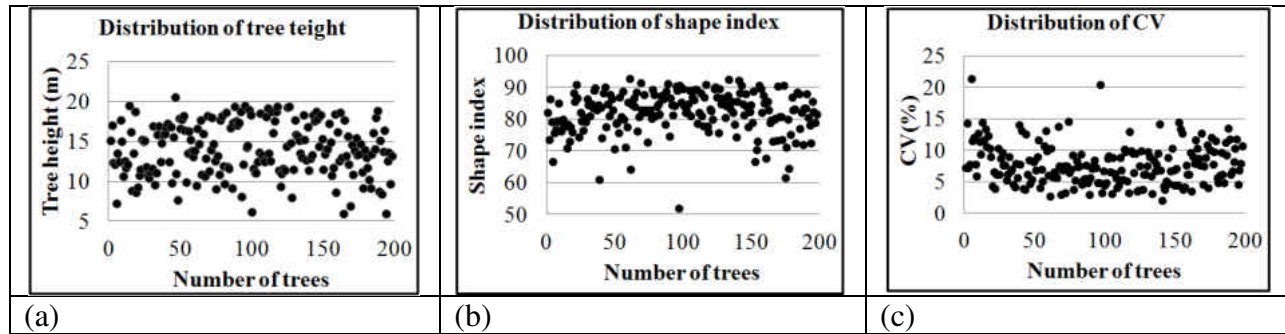
Figure 17 Structure features. Tree height (a), shape index (b),and coefficient of variation (c).

4.4.3 Spectral feature extraction from AISA hyperspectral imagery

To reduce the dimensionality of the hyperspectral data, the stepwise spectral discriminant analysis (SDA) was applied to both treetop-based and pixel-weighted spectra. Based on Wilk's lambda values, 6 optimal bands from the treetop-based spectra and 9 optimal bands from the pixel-weighted spectra were identified at a 5% level of significance. Of the 6 optimal treetop-based bands, 1 band was from the visible region, 2 bands from VNIR, and 3 bands from SWIR. Of the 9 optimal pixel-weighted bands, 2 bands were from the visible region, 6 bands from VNIR, and 1 band from SWIR.

To assess the lost information in selecting optimal bands, both full bands and optimal bands were used to classify tree species with the same samples and SVM algorithms. The results indicate that the classified map using 6 optimal bands matches 95.08% with the classified map using all 312 treetop-based bands. The 6 bands with SVM resulted in 66.45% of overall accuracy with 0.52 of kappa statistics, while all 312 bands with SVM resulted in 68.38% of overall accuracy with 0.54 of kappa statistics. Similarly, the classified map using 9 optimal bands matches 99.85% with the classified map using all 312 pixel-weighted bands. The overall accuracy using 9 optimal bands is the same as that using all 312 pixel-weighted bands (80.64%) and their kappa statistics were almost the same (0.7186 and 0.7197). Since optimal bands and all

bands produced similar classification results, 6 and 9 optimal bands were taken up for further treetop-based classification and pixel-weighting classification.

4.4.4   Classification results

The accuracies of treetop-based classification with four combined subsets were summarized in Table 8. The spectral only variables resulted in an overall accuracy of 66.45% and kappa statistics of 0.52. The producer's accuracies ranged from 43.59% to 78.57%, and the user's accuracy are from 57.89% to 77.27%. Adding tree height information into the SVM classification reduced the overall accuracy to 64.52% and kappa statistics to 0.49. The highest producer's accuracy decreased to 74.36% from 78.57% and the highest user's accuracy decreased to 50.00% from 77.27%. In contrast, joining crown shape index into the classification increased the overall accuracy to 71.61% and kappa statistics to 0.60. Furthermore, including coefficient of variation as classification input increased the overall accuracy to 72.90% and kappa statistics to 0.61. Specifically, the highest producer's accuracy reached 82.05% for ash tree species and highest user's accuracy reached 79.07% for maple tree species.

Table 8 Accuracy comparison on treetop-based fusion

Species	Spectral only		Spectral + TH		Spectral + SI		Spectral + CV	
	Prod. (%)	User (%)	Prod. (%)	User (%)	Prod. (%)	User (%)	Prod. (%)	User (%)
Ash	43.59	73.91	74.36	64.44	79.49	72.09	82.05	76.19
Maple	72.34	77.27	68.09	68.09	72.34	72.27	72.34	79.07
Oak	78.57	57.89	66.07	62.71	71.43	67.80	75.00	66.67
Other	61.54	66.67	15.38	50.00	46.15	66.67	38.46	71.43
OA	66.45		64.52		71.61		72.90	
Kappa	0.52		0.49		0.60		0.61	

Pixel-weighting approach improved the classification results (see Table 9). With weighted spectra only, the overall accuracy increased to 80.64% and the kappa statistics increased to 0.72.

The three dominate trees: ash, maple, and oak were mapped with producer's accuracies from

82.98% to 89.29% and the user's accuracies from 72.46% to 86.67%. The impacts of the three

structural features in pixel-weighting approach are similar to those in the treetop-based approach,

but the magnitudes of their contributions are different. The addition of the LiDAR derived tree

height decreased the overall accuracy to 71.61% and kappa statistics to 0.59. Specific to the three

dominate tree species, their producer's accuracies decreased 12.83%, 17.02%, and 1.79% and the

user's accuracies decreased 6.84%, 19.28%, and 2.26% from using only spectral data

respectively. However, the crown shape and height dispersion information improved the

classification results. With shape index, the overall accuracy increased to 81.29% and kappa

statistics increased to 0.73. In specific, increases in producer's and user's accuracies were

observed for ash (84.62% and 91.67%), for maple (82.98% and 82.98%), and for oak (92.86%

and 74.29%). Similarly, the combination of hyperspectral and CV data increased the overall

accuracy to 81.94% and kappa statistics to 0.74. The notable increases in producer's and user's

accuracies occurred for ash (92.31% and 87.80%), maple (78.72% and 90.24%), and oak

(89.29% and 74.63%).

Table 9 Accuracy comparison on weighted pixel based fusion

Species	Spectral only		Spectral + tree		Spectral + SI		Spectral + CV	
	Prod. (%)	User (%)	Prod. (%)	User (%)	Prod. (%)	User (%)	Prod. (%)	User (%)
Ash	84.62	86.84	71.79	80.00	84.62	91.67	92.31	87.80
Maple	82.98	86.67	65.96	67.39	82.98	82.98	78.72	90.24
Oak	89.29	72.46	87.50	70.00	92.86	74.29	89.29	74.63
Other	23.08	100.00	23.08	75.00	15.38	100.00	30.77	66.67
OA	80.64		71.61		81.29		81.94	
Kappa	0.72		0.59		0.73		0.74	

4.4.5 Discussion

Data fusion, especially the fusion of hyperspectral imagery and high density LiDAR data, has become attractive to improve tree species classification. On one hand, the over-determined spectral signature of hyperspectral data measures more accurate and detailed spectral information related to biochemical features (Lee et al., 2004) and drives tree species classification at different conditions (Ghosh et al., 2014). On the other hand, LiDAR data allows for the measurement of crown structural properties (e.g. tree height and crown size) and provides complimentary information to hyperspectral imagery to mitigate the spectral similarity problem for different tree species (Leckie et al., 2005). However, the magnitude of LiDAR data contribution depends on structural feature selection. The same tree species may exhibit different biophysical properties while the different tree species may have similar physical dimensions. Therefore, selection the optimal structural feature insensitive to the tree's life cycle and living environments is a critical task.

Regarding the contributions of the three structure features, tree height decreased the classification accuracy, but the shape information and dispersion variables increased the classification results. The study area is dominated by the deciduous trees, such as ash, maple, oak, and honey locust. The same species may exhibit different heights at different ages, while different species may have similar heights. Therefore, the variation within a species is high, and the variation between species is relatively low (e.g. standard deviation within ash species (2.31m) to standard deviation between species (3.29 m)) (see Figure 18a). Therefore, the confusion of tree heights reduced the overall accuracies of tree species discrimination with either treetop-based or pixel-weighting classification. Although tree height information with treetop-based classification increased producer's accuracy for ash tree species (from 43.59% to 74.36%)

and user's accuracy for oak species (from 57.89% to 62.71%), it decreased the producer's and user's accuracies for other species. The absolute tree heights may provide complementary information for tree species classification in singularly dominant age classes, but they have little contributions for the classification in a forest with multiple age classes, especially for deciduous species, which is consistent with the results presented by Jones et al. (2010).

In comparison with the tree height variable, the shape information provides more explanatory power for deciduous tree species classification. Crown shape is an important structural characteristic which is related to radiation absorption, photosynthesis, and transpiration (Wang and Jarvis, 1990). Zeide and Pfeifer (1991) further pointed out the same species have geometrically similar crown shapes, so incorporating tree crown shape information can improve classification performance (Kulikova et al., 2007). In this study, shape index is proved to be effective in characterizing the four species. The fusion shape index and treetop-based spectra raised the overall accuracy to 71.61% and kappa statistics to 0.60, while the fusion of shape index and pixel-weighted bands raised the overall accuracy to 81.29% and kappa statistics to 0.73. The contribution of shape information comes from lower ratio of variations within-species to between-species as compared to the height information. For example, the standard deviation within ash species is 3.45 while the standard deviation between species is 6.58 (see Figure 18b).

CV performs slightly better than shape index in improving the species classification. By integrating CV, treetop-based classification increased the overall accuracy to72.9% from that with treetop-based spectra only (66.45%), while the pixel-weighting classification increased the overall accuracy to 81.94% from that with pixel-weighted spectra only (80.64%). CV is a normalized measure of dispersion of the probability distribution and therefore is employed to compare datasets with significantly different means. Similar to shape index, lower within-species

variation to higher between-species variation contributes to higher accuracy of species

classification. As an example, the standard deviation of ash species is 1.69 while the between-

species value is 3.19 (see Figure 18c). Thus, for e ash trees, adding CV into treetop-based

classification increased producer's accuracy to 82.05% and user's accuracy to 76.19%, while

including CV as classification input of pixel-weighting classification increased producer's

accuracy to 92.31% and user's accuracy to 87.80%.
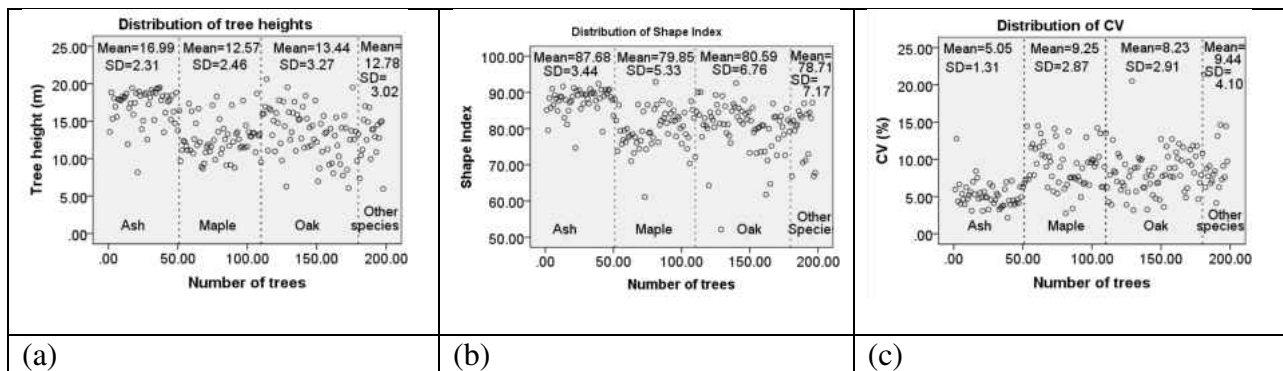
Figure 18 Distribution of tree height (a), shape index (b), and CV (c).

From our experiment, the contribution of LiDAR data to treetop-based classification is

higher than that to pixel-weighting classification. Since treetop spectra are still impacted by pixel

mixture problems and exhibit spectral confusion, the spectral similarity of treetop pixels

decreases classification accuracy. In contrast, the structural features, such as shape information

and height dispersion within a crown, have the ability to characterize the distinct crown

morphology. Therefore, incorporating these structure features can increase accuracy for

classifying different species which exhibit similar spectral properties (Jones et al., 2010).

However, pixel-weighting approach extracted the relative pure crown-scale spectra, and tree

species have already been well characterized with the pure hyperspectral information. Thus, less

information is needed from LiDAR data to complement the species classification.

4.5 Conclusion

This research sought to improve species mapping in deciduous dominated urban forests by fusing hyperspectral imagery and LiDAR data. Treetop-based spectra avoid the interference from other materials around the overlapping crown boundaries and pixel-weighted spectra suffer less mixed-pixel problems, but spectral confusion still existed in a biodiverse forest. LiDAR data provide additional power in improving classification accuracy for tree species with distinct structures but similar spectral properties. Three structure features: tree height, crown shape index, and coefficient of variation within tree crowns were extracted and integrated with treetop-based and pixel-weighted crown spectra respectively. Results suggest crown shape and height dispersion information increase the classification accuracy because they can measure the complex biophysical properties, but tree height decreases the accuracy due to simple information extraction.

Shape signature illustrates the probability distribution of heights for random points within a crown and shape index further expresses the shape signature of a 3D object in one dimension (1D). Through extracting the shape signature and calculating the shape index from LiDAR data, 3D shape matching problems were reduced to 2D probability distributions and further to the simple 1D index value. The results indicate that the shape index is efficient in computation and effective in representing a complex crown shape. CV refers to a standardized measure of height dispersion within a crown and represents the ratio of the standard derivation to the mean. Thus it is suitable for comparing data sets with different means and different measures. As a result, integrating with shape index and CV respectively, both the treetop-based and pixel-weighting approaches increased the classification accuracies, but CV performs better than shape index

because CV measures the degree of height dispersion while shape index only expresses the trends of height distribution.

Pixel-weighted spectra outperform treetop-based spectra in the fusion with shape-related structural features for tree species classification. Treetop-based spectra exhibit spectral confusion due to spectral mixture problem in biodiverse forest, so the hyperspectral only resulted in lower classification results (66.45% overall accuracy). Adding the structural features, the overall accuracy increased to 71.61% with shape index and 72.90% with CV respectively. In contrast, relative pure crown spectra extracted using pixel-weighting approach well characterized the species and classified the species with high accuracy (80.64%). Moreover, the pixel-weighted spectra/shape index fusion increased the overall accuracy to 81.29% and the pixel-weighted spectra/CV fusion increased the overall accuracy to 81.94%.

Tree species classification in deciduous forests is challenging. The spectral similarity amongst different species and spectral noise caused by mixed-pixel problem decrease the accuracy of tree species classification. However, the appropriate structural features (e.g. SI and CV) extracted from LiDAR data have the ability to measure unique crown biophysical properties invariable from life stage and mitigate the spectral problems. Therefore, the fusion of the hyperspectral imagery and LiDAR data can improve the tree species classification.

Acknowledgements

CHAPTER 5 CONCLUSIONS

5.1 Summary

Crown-level tree species classification in urban areas is essential for forest inventory and resource evaluation. Specifically, ash tree identification in Milwaukee is critical in the management of the pest of EAB to prevent a loss of ash canopy and associated environmental benefits. However, the crown-level species classification from remote sensing imagery is a challenging task due to spectral similarity and spatial proximity. Moreover, shadow, gaps, double-side illumination, and other materials in the crown area may influence the crown-scale spectral extraction, the age and canopy architecture may influence the crown size estimation of a tree species. To address these issues, this research integrated hyperspectral imagery and discrete-return LiDAR data to improve the crown-level tree species classification. The hyperspectral imagery measures detailed spectral reflectance related to the biochemical properties of vegetation, while LiDAR data measures the three-dimensional structure of tree crowns related to morphological characteristics. Specifically, three new approaches have been proposed for canopy delineation, pure crown-scale spectral computation, and structure characteristic extraction respectively. First, a general geometric model was generated by optimally fitting the crown surface to extract the crown variables and then a regression model was developed to estimate the crown width for canopy delineation. Second, a pixel-weighting approach was developed to calculate the pure crown-scale spectra and SVM classifier was used to classify the species with high overall accuracy. Finally, crown shape related variables were extracted from LiDAR derived canopy height model and fused with spectral data for tree species classification.

5.2 Contributions

The first contribution of this research is the automated delineation of individual tree crowns from LiDAR data by combining a generalized geometric model and a regression model. The canopy height model derived from LiDAR data or optical imagery can be segmented to obtain individual tree crowns. However, the ambiguous crown boundaries caused by overlapping branches and canopy gaps within a tree crown make current individual tree crown delineation methods work less effectively on closed canopy mixed wood forests. In contrast, the generalized geometric model can address these problems by optimally fitting the crown surface, as the model shows clear crown boundaries and distinct tops. Moreover, the generalized geometric model has the ability to simulate different crown shapes, such as cones, semi-spheres, half-ellipsoids as well as other shapes, and extract shape related parameters, such as curvature and curvature coefficient. Thereafter, a linear regression analysis model, using these LiDAR derived tree height and shape related parameters as independent variables, was designed to estimate the tree crown width. Statistical analysis indicates that there is a very strong relationship between the crown width and the variables extracted from the geometric model. Therefore, the integration of the generalized geometric model and linear regression model facilitates the automated crown segmentation.

The second contribution of this research is the computation of the relative pure spectral reflectance at the crown level for the improved tree species classification. High purity of reflectance spectra is proved to contribute to high accuracies of tree species classifications. However, mixed-pixels and pixels under different illumination conditions are very common within crowns. Thus, the traditional method of calculating the crown-scale spectra, averaging pixel spectra within a crown, blurs within-crown variations and further decreases the species

classification accuracy. To address this issue, the pixel-weighting algorithm was developed in this research to extract the relative pure crown-scale spectra. Specifically, the illuminated-leaf fraction of each pixel was first extracted using a constrained linear SMA, and then the pure crown-scale spectra was calculated by weighted averaging all pixel spectra within the crown area using their illuminated-leaf fractions as weights. The pixel-weighted spectra not only measure the unique spectral characteristic of a species at the individual tree level, but also resist the impacts from crown delineation error and spectral outliers. Working with the SVM classifier, pixel-weighted crown-scale spectra produced higher classification accuracies than treetop-based classification and pixel-majority classification.

The third contribution of this research is the extraction of shaped-related structural features as well as fusion of the structural and spectral features for tree species classification. Urban forests are dynamic and complicated ecosystems due to the constant tree growth and species diversity. Thus the canopy height model and simple height metric have the limitation in displaying the crown structural features. In contrast, the shape-related structural features are basically consistent to life stages and able to capture between species variability in crown morphology. Therefore, both shape index and coefficient of variation were extracted from LiDAR derived CHM to express the height distribution and height dispersion within a crown. These two indices avoid the influence of absolute tree heights and canopy architectures, so they have the potential to represent the unique crown structural characteristics of tree species and play an important role in tree species classification.

When crown-scale spectra were extracted from the hyperspectral imagery and structural metrics were extracted from LiDAR data, these two spatial and spectral features were integrated for ash tree identification. The relative pure crown-scale spectra capture subtle differences in

spectral characteristics while the LiDAR features including shape index and CV describe the unique crown structural characteristics. Therefore, the integration of LiDAR data and hyperspectral imagery at the individual tree level is effective in improving tree species identification.

5.3 Future research

Future research will be focusing on two aspects. The first is the generation of a Triangular Irregular Networks (TIN) based model of forest canopy for crown segmentation and shape variables extraction. Grid models like CHM are the most frequently used model in forest study due to their ease of storage and manipulate, fast computation, and smooth appearance of the canopy surface. However, the fixed-resolution in the grid system does not adapt to the variability of terrain, and the grid values do not reflect the actual measurements due to the absence of source data in the interpolation process. In contrast, TINs are vector-based representations of a surface as a set of continuous and non-overlapping triangles. The detailed relief information of a complex surface can be captured because the variable-resolution is adapted to the variability of terrain. Moreover, there is no information lost because source data is maintained as part of triangulation. Therefore, with the TIN-based model, the accurate crown segmentation can be conducted and correct shape variables can be extracted. The second aspect is the application of the phenology to assist hyperspectral species classification. The tree species classification using hyperspectral imagery is a challenge due to the similar spectral reflectance between different tree species. However, the different vegetation can be characterized by different features of growth trajectory and phenology. The tree species with similar phenological characteristics from green-up to senescence can be considered as the same ones. Therefore, multi-temporal images provide the potential of classifying the tree species using time series of spectral variable.

References

Adams, J.B., Sabol, D.E., Kapos, V., Almeida Filho, R., Roberts, D.A., Smith, M.O., & Gillespie, A.R. (1995). Classification of multispectral images based on fractions of endmembers: Application to land-cover change in the Brazilian Amazon. *Remote Sensing of environment, 52*, 137-154

Akbari, H. (2002). Shade trees reduce building energy use and CO 2 emissions from power plants. *Environmental pollution, 116*, S119-S126

Alonzo, M., Bookhagen, B., & Roberts, D.A. (2014). Urban tree species mapping using hyperspectral and lidar data fusion. *Remote Sensing of environment, 148*, 70-83

Alonzo, M., Roth, K., & Roberts, D. (2013). Identifying Santa Barbara's urban tree species from AVIRIS imagery using canonical discriminant analysis. *Remote Sensing Letters, 4*, 513-521

Alvey, A.A. (2006). Promoting and preserving biodiversity in the urban forest. *Urban Forestry & Urban Greening, 5*, 195-201

Armson, D., Stringer, P., & Ennos, A. (2012). The effect of tree shade and grass on surface and globe temperatures in an urban area. *Urban Forestry & Urban Greening, 11*, 245-255

Armson, D., Stringer, P., & Ennos, A. (2013). The effect of street trees and amenity grass on urban surface water runoff in Manchester, UK. *Urban Forestry & Urban Greening, 12*, 282-286

Bai, L., Lin, H., Sun, H., Mo, D., & Yan, E. (2012). Spectral Unmixing Approach in Remotely Sensed Forest Cover Estimation: A Study of Subtropical Forest in Southeast China. *Physics Procedia, 25*, 1055-1062

Baldeck, C.A., Asner, G.P., Martin, R.E., Anderson, C.B., Knapp, D.E., Kellner, J.R., & Wright, S.J. (2015). Operational tree species mapping in a diverse tropical forest with airborne imaging spectroscopy. *PloS one, 10*, e0118403

Banskota, A., Wynne, R.H., & Kayastha, N. (2011). Improving within-genus tree species discrimination using the discrete wavelet transform applied to airborne hyperspectral data. *International Journal of Remote Sensing, 32*, 3551-3563

Ben-Arie, J.R., Hay, G.J., Powers, R.P., Castilla, G., & St-Onge, B. (2009). Development of a pit filling algorithm for LiDAR canopy height models. *Computers & Geosciences, 35*, 1940-1949

Biging, G.S., & Dobbertin, M. (1995). Evaluation of competition indices in individual tree growth models. *Forest Science, 41*, 360-377

Bishop, B.D., Dietterick, B.C., White, R.A., & Mastin, T.B. (2014). Classification of Plot-Level Fire-Caused Tree Mortality in a Redwood Forest Using Digital Orthophotography and LiDAR. *Remote Sensing, 6*, 1954-1972

Blanusa, T., Fantozzi, F., Monaci, F., & Bargagli, R. (2015). Leaf trapping and retention of particles by holm oak and other common tree species in Mediterranean urban environments. *Urban Forestry & Urban Greening, 14*, 1095-1101

Brandtberg, T. (1999). Automatic individual tree based analysis of high spatial resolution aerial images on naturally regenerated boreal forests. *Canadian Journal of Forest Research, 29*, 1464-1478

Cappaert, D., McCullough, D.G., Poland, T.M., & Siegert, N.W. (2005). Emerald ash borer in North America: a research and regulatory challenge. *American Entomologist, 51*, 152-165

Carlson, K.M., Asner, G.P., Hughes, R.F., Ostertag, R., & Martin, R.E. (2007). Hyperspectral remote sensing of canopy biodiversity in Hawaiian lowland rainforests. *Ecosystems, 10*, 536-549

Castrillo, L.A., Griggs, M.H., & Vandenberg, J.D. (2008). Quantitative detection of Beauveria bassiana GHA (Ascomycota: Hypocreales), a potential microbial control agent of the emerald ash borer, by use of real-time PCR. *Biological Control, 45*, 163-169

Charaniya, A.P., Manduchi, R., & Lodha, S.K. (2004). Supervised parametric classification of aerial lidar data. In, *Computer Vision and Pattern Recognition Workshop, 2004. CVPRW'04. Conference on* (pp. 30-30): IEEE

Chen, Q., Baldocchi, D., Gong, P., & Kelly, M. (2006). Isolating individual trees in a savanna woodland using small footprint lidar data. *Photogrammetric Engineering & Remote Sensing, 72*, 923-932

Chen, W.Y., & Wang, D.T. (2013). Urban forest development in China: Natural endowment or socioeconomic product? *Cities, 35*, 62-68

Cilliers, S. (2010). Social aspects of urban biodiversity–An overview. In, *N. Müller, P. Werner & J. Kelcey, Urban biodiversity and design—implementing the convention on biological diversity in towns and cities* (pp. 81-100)

Clark, M.L., & Roberts, D.A. (2012). Species-level differences in hyperspectral metrics among tropical rainforest trees as determined by a tree-based classifier. *Remote Sensing, 4*, 1820-1855

Clark, M.L., Roberts, D.A., & Clark, D.B. (2005). Hyperspectral discrimination of tropical rain forest tree species at leaf to crown scales. *Remote Sensing of environment, 96*, 375-398

Clark, M.L., Roberts, D.A., Ewel, J.J., & Clark, D.B. (2011). Estimation of tropical rain forest aboveground biomass with small-footprint lidar and hyperspectral sensors. *Remote Sensing of environment, 115*, 2931-2942

Cochrane, M. (2000). Using vegetation reflectance variability for species level classification of hyperspectral data. *International Journal of Remote Sensing, 21*, 2075-2087

Colditz, R., Schmidt, M., Conrad, C., Hansen, M., & Dech, S. (2011). Land cover classification with coarse spatial resolution data to derive continuous and discrete maps for complex regions. *Remote Sensing of environment, 115*, 3264-3275

Conway, T.M., & Vander Vecht, J. (2015). Growing a diverse urban forest: Species selection decisions by practitioners planting and supplying trees. *Landscape and Urban Planning, 138*, 1-10

Cristiano, P.M., Madanes, N., Campanello, P.I., di Francescantonio, D., Rodríguez, S.A., Zhang, Y.-J., Carrasco, L.O., & Goldstein, G. (2014). High NDVI and potential canopy photosynthesis of South American subtropical forests despite seasonal changes in Leaf Area Index and air temperature. *Forests, 5*, 287-308

Dalponte, M., Bruzzone, L., & Gianelle, D. (2008). Fusion of hyperspectral and LIDAR remote sensing data for classification of complex forest areas. *Geoscience and Remote Sensing, IEEE Transactions on, 46*, 1416-1427

Dalponte, M., Bruzzone, L., & Gianelle, D. (2009). Fusion of hyperspectral and lidar remote sensing data for the estimation of tree stem diameters. In, *Geoscience and Remote Sensing Symposium, 2009 IEEE International, IGARSS 2009* (pp. II-1008-II-1011): IEEE

Dalponte, M., Bruzzone, L., & Gianelle, D. (2012). Tree species classification in the Southern Alps based on the fusion of very high geometrical resolution multispectral/hyperspectral images and LiDAR data. *Remote Sensing of environment, 123*, 258-270

Dalponte, M., Orka, H.O., Gobakken, T., Gianelle, D., & Næsset, E. (2013). Tree species classification in boreal forests with hyperspectral data. *Geoscience and Remote Sensing, IEEE Transactions on, 51*, 2632-2645

Deng, S., Shi, Y., Jin, Y., & Wang, L. (2011). A GIS-based approach for quantifying and mapping carbon sink and stock values of forest ecosystem: a case study. *Energy Procedia, 5*, 1535-1545

Dong, P. (2009). Characterization of individual tree crowns using three-dimensional shape signatures derived from LiDAR data. *International Journal of Remote Sensing, 30*, 6621-6628

Doruska, P.F., & Burkhart, H.E. (1994). Modeling the diameter and locational distribution of branches within the crowns of loblolly pine trees in unthinned plantations. *Canadian Journal of Forest Research, 24*, 2362-2376

Fauvel, M., Benediktsson, J.A., Chanussot, J., & Sveinsson, J.R. (2008). Spectral and spatial classification of hyperspectral data using SVMs and morphological profiles. *IEEE Transactions on Geoscience and Remote Sensing, 46*, 3804-3814

Flower, C.E., Knight, K.S., & Gonzalez-Meler, M.A. (2013). Impacts of the emerald ash borer (Agrilus planipennis Fairmaire) induced ash (Fraxinus spp.) mortality on forest carbon cycling and successional dynamics in the eastern United States. *Biological Invasions, 15*, 931-944

Gatziolis, D., & Andersen, H.-E. (2008). *A guide to LIDAR data acquisition and processing for the forests of the Pacific Northwest*. US Department of Agriculture, Forest Service, Pacific Northwest Research Station

George, R., Padalia, H., & Kushwaha, S. (2014). Forest tree species discrimination in western Himalaya using EO-1 Hyperion. *International Journal of Applied Earth Observation and Geoinformation, 28*, 140-149

Ghosh, A., Fassnacht, F.E., Joshi, P., & Koch, B. (2014). A framework for mapping tree species combining hyperspectral and LiDAR data: Role of selected classifiers and sensor across three spatial scales. *International Journal of Applied Earth Observation and Geoinformation, 26*, 49-63

Gill, S.J., Biging, G.S., & Murphy, E.C. (2000). Modeling conifer tree crown radius and estimating canopy cover. *Forest Ecology and Management, 126*, 405-416

Goddard, M.A., Dougill, A.J., & Benton, T.G. (2010). Scaling up from gardens: biodiversity conservation in urban environments. *Trends in Ecology & Evolution, 25*, 90-98

Godwin, C., Chen, G., & Singh, K.K. (2015). The impact of urban residential development patterns on forest carbon density: An integration of LiDAR, aerial photography and field mensuration. *Landscape and Urban Planning, 136*, 97-109

Gong, P., Pu, R., & Yu, B. (1997). Conifer species recognition: an exploratory analysis of in situ hyperspectral data. *Remote Sensing of environment, 62*, 189-200

Gougeon, F.A. (1995). A crown-following approach to the automatic delineation of individual tree crowns in high spatial resolution aerial images. *Canadian journal of remote sensing, 21*, 274-284

Gougeon, F.A., Leckie, D.G., Paradine, D., & Scott, I. (1999). Individual tree crown species recognition: The Nahmint study. *Automated interpretation of high spatial resolution digital imagery for forestry*, 209-223

Green, R.O., Eastwood, M.L., Sarture, C.M., Chrien, T.G., Aronsson, M., Chippendale, B.J., Faust, J.A., Pavri, B.E., Chovit, C.J., & Solis, M. (1998). Imaging spectroscopy and the airborne visible/infrared imaging spectrometer (AVIRIS). *Remote Sensing of environment, 65*, 227-248

Harlow, W.M. (1991). *Textbook of dendrology: Covering the important forest trees of the United States and Canada*. McGraw-Hill

Heinzel, J., & Koch, B. (2012). Investigating multiple data sources for tree species classification in temperate forest and use for single tree delineation. *International Journal of Applied Earth Observation and Geoinformation, 18*, 101-110

Herms, D., Bonello, P., Smitley, D., Rebek, E., & Cipollini, D. (2004). Interspecific variation in ash resistance/susceptibility to EAB. In, *2004 Annual Emerald Ash Borer Meeting, Romulus, Michigan, USA, October*

Hill, R., & Thomson, A. (2005). Mapping woodland species composition and structure using airborne spectral and LiDAR data. *International Journal of Remote Sensing, 26*, 3763-3779

Holmgren, J., Nilsson, M., & Olsson, H. (2003). Estimation of tree height and stem volume on plots using airborne laser scanning. *Forest Science, 49*, 419-428

Holmgren, P., & Thuresson, T. (1998). Satellite remote sensing for forestry planning—a review. *Scandinavian Journal of Forest Research, 13*, 90-110

Hu, B., Li, J., Jing, L., & Judah, A. (2014). Improving the efficiency and accuracy of individual tree crown delineation from high-density LiDAR data. *International Journal of Applied Earth Observation and Geoinformation, 26*, 145-155

Hughes, G.P. (1968). On the mean accuracy of statistical pattern recognizers. *Information Theory, IEEE Transactions on, 14*, 55-63

Huguenin, R.L., Karaska, M.A., Van Blaricom, D., & Jensen, J.R. (1997). Subpixel classification of bald cypress and tupelo gum trees in Thematic Mapper imagery. *Photogrammetric Engineering and Remote Sensing, 63*, 717-724

Hyyppä, J., & Inkinen, M. (1999). Detecting and estimating attributes for single trees using laser scanner. *The photogrammetric journal of Finland, 16*, 27-42

Hyyppä, J., Pyysalo, U., Hyyppä, H., & Samberg, A. (2000). Elevation accuracy of laser scanning-derived digital terrain and target models in forest environment. In, *Proceedings of EARSeL-SIG-Workshop LIDAR* (pp. 14-17)

Jonckheere, I., Fleck, S., Nackaerts, K., Muys, B., Coppin, P., Weiss, M., & Baret, F. (2004). Review of methods for in situ leaf area index determination: Part I. Theories, sensors and hemispherical photography. *Agricultural and forest meteorology, 121*, 19-35

Jones, T.G., Coops, N.C., & Sharma, T. (2010). Assessing the utility of airborne hyperspectral and LiDAR data for species distribution mapping in the coastal Pacific Northwest, Canada. *Remote Sensing of environment, 114*, 2841-2852

Kato, A., Moskal, L.M., Schiess, P., Swanson, M.E., Calhoun, D., & Stuetzle, W. (2009). Capturing tree crown formation through implicit surface reconstruction using airborne lidar data. *Remote Sensing of environment, 113*, 1148-1162

Kendal, D., Dobbs, C., & Lohr, V.I. (2014). Global patterns of diversity in the urban forest: Is there evidence to support the 10/20/30 rule? *Urban Forestry & Urban Greening, 13*, 411-417

Koch, B., Heyder, U., & Weinacker, H. (2006). Detection of individual tree crowns in airborne lidar data. *Photogrammetric Engineering & Remote Sensing, 72*, 357-363

KOCH, V.B., Svoboda, J., Adler, P., & Dees, M. (2002). Automatische baumartenerkennung auf der Grundlage digitalisierter CIR-luftbilder. *173. JAHRGANG 2002 HEFT 7/8 JULI/AUGUST JD SAUERLANDER'S VERLAG· FRANKFURT AM MAIN*, 131

Koetz, B., Morsdorf, F., Van der Linden, S., Curt, T., & Allgöwer, B. (2008). Multi-source land cover classification for forest fire management based on imaging spectrometry and LiDAR data. *Forest Ecology and Management, 256*, 263-271

Konijnendijk, C.C., Ricard, R.M., Kenney, A., & Randrup, T.B. (2006). Defining urban forestry—A comparative perspective of North America and Europe. *Urban Forestry & Urban Greening, 4*, 93-103

Kovacs, K.F., Haight, R.G., McCullough, D.G., Mercader, R.J., Siegert, N.W., & Liebhold, A.M. (2010). Cost of potential emerald ash borer damage in US communities, 2009–2019. *Ecological Economics, 69*, 569-578

Kulikova, M.S., Mani, M., Srivastava, A., Descombes, X., & Zerubia, J. (2007). Tree species classification using radiometry, texture and shape based features. In, *Signal Processing Conference, 2007 15th European* (pp. 1595-1599): IEEE

Leckie, D., Gougeon, F., Hill, D., Quinn, R., Armstrong, L., & Shreenan, R. (2003). Combined high-density lidar and multispectral imagery for individual tree crown analysis. *Canadian journal of remote sensing, 29*, 633-649

Leckie, D.G., Tinis, S., Nelson, T., Burnett, C., Gougeon, F.A., Cloney, E., & Paradine, D. (2005). Issues in species classification of trees in old growth conifer stands. *Canadian journal of remote sensing, 31*, 175-190

Lee, K.-S., Cohen, W.B., Kennedy, R.E., Maiersperger, T.K., & Gower, S.T. (2004). Hyperspectral versus multispectral data for estimating leaf area index in four different biomes. *Remote Sensing of environment, 91*, 508-520

Lefsky, M.A., Cohen, W.B., Parker, G.G., & Harding, D.J. (2002). Lidar Remote Sensing for Ecosystem Studies Lidar, an emerging remote sensing technology that directly measures the three-dimensional distribution of plant canopies, can accurately estimate vegetation structural attributes and should be of particular interest to forest, landscape, and global ecologists. *BioScience, 52*, 19-30

Li, J., Hu, B., & Noland, T.L. (2013). Classification of tree species based on structural features derived from high density LiDAR data. *Agricultural and forest meteorology, 171*, 104-114

Li, W., Guo, Q., Jakubowski, M.K., & Kelly, M. (2012). A new method for segmenting individual trees from the lidar point cloud. *Photogrammetric Engineering & Remote Sensing, 78*, 75-84

Lim, K., Treitz, P., Baldwin, K., Morrison, I., & Green, J. (2003). Lidar remote sensing of biophysical properties of tolerant northern hardwood forests. *Canadian journal of remote sensing, 29*, 658-678

Liu, H., & Dong, P. (2014). A new method for generating canopy height models from discrete-return LiDAR point clouds. *Remote Sensing Letters, 5*, 575-582

Liu, H., & Wu, C. (2016). Tree Crown Width Estimation Using Discrete Airborne LiDAR Data. *Canadian journal of remote sensing*, 00-00

Liu, J., Shen, J., Zhao, R., & Xu, S. (2013). Extraction of individual tree crowns from airborne LiDAR data in human settlements. *Mathematical and Computer Modelling, 58*, 524-535

Liu, L., Pang, Y., Fan, W., Li, Z., & Li, M. (2011). Fusion of airborne hyperspectral and LiDAR data for tree species classification in the temperate forest of northeast China. In, *Geoinformatics, 2011 19th International Conference on* (pp. 1-5): IEEE

Lu, D., & Weng, Q. (2004). Spectral mixture analysis of the urban landscape in Indianapolis with Landsat ETM+ imagery. *Photogrammetric Engineering & Remote Sensing, 70*, 1053-1062

Lu, D., & Weng, Q. (2007). A survey of image classification methods and techniques for improving classification performance. *International Journal of Remote Sensing, 28*, 823-870

MacFarlane, D.W., & Meyer, S.P. (2005). Characteristics and distribution of potential ash tree hosts for emerald ash borer. *Forest Ecology and Management, 213*, 15-24

Maclean, G.A., & Krabill, W. (1986). Gross-merchantable timber volume estimation using an airborne LIDAR system. *Canadian journal of remote sensing, 12*, 7-18

Manes, F., Incerti, G., Salvatori, E., Vitale, M., Ricotta, C., & Costanza, R. (2012). Urban ecosystem services: tree diversity and stability of tropospheric ozone removal. *Ecological Applications, 22*, 349-360

Manes, F., Seufert, G., & Vitale, M. (1997). Ecophysiological studies of Mediterranean plant species at the Castelporziano estate. *Atmospheric Environment, 31*, 51-60

Martin, M., Newman, S., Aber, J., & Congalton, R. (1998). Determining forest species composition using high spectral resolution remote sensing data. *Remote Sensing of environment, 65*, 249-254

Mate, R., Johansson, T., & Sitoe, A. (2014). Biomass equations for tropical forest tree species in Mozambique. *Forests, 5*, 535-556

McKenney, D.W., Pedlar, J.H., Yemshanov, D., Barry Lyons, D., Campbell, K.L., & Lawrence, K. (2012). Estimates of the potential cost of emerald ash borer (Agrilus planipennis Fairmaire) in Canadian municipalities. *Arboriculture and Urban Forestry, 38*, 81

Meddens, A.J., Hicke, J.A., & Vierling, L.A. (2011). Evaluating the potential of multispectral imagery to map multiple stages of tree mortality. *Remote Sensing of environment, 115*, 1632-1642

Morsdorf, F., Kötz, B., Meier, E., Itten, K., & Allgöwer, B. (2006). Estimation of LAI and fractional cover from small footprint airborne laser scanning data based on gap fraction. *Remote Sensing of environment, 104*, 50-61

Morsdorf, F., Meier, E., Allgöwer, B., & Nüesch, D. (2003). Clustering in airborne laser scanning raw data for segmentation of single trees. *International Archives of the Photogrammetry, Remote Sensing and Spatial Information Sciences, 34*, W13

Morsdorf, F., Meier, E., K∀∂tz, B., Itten, K.I., Dobbertin, M., & Allg∀∂wer, B. (2004). LIDAR-based geometric reconstruction of boreal type forest stands at single tree level for forest and wildland fire management. *Remote Sensing of environment, 92*, 353-362

Mullaney, J., Lucke, T., & Trueman, S.J. (2015). A review of benefits and challenges in growing street trees in paved urban environments. *Landscape and Urban Planning, 134*, 157-166

Naesset, E. (1997). Determination of mean tree height of forest stands using airborne laser scanner data. *ISPRS Journal of Photogrammetry and Remote Sensing, 52*, 49-56

Næsset, E., & Økland, T. (2002). Estimating tree height and tree crown properties using airborne scanning laser in a boreal nature reserve. *Remote Sensing of environment, 79*, 105-115

Nguyen, T., Yu, X., Zhang, Z., Liu, M., & Liu, X. (2015). Relationship between types of urban forest and PM 2.5 capture at three growth stages of leaves. *Journal of Environmental Sciences, 27*, 33-41

Nilsson, M. (1996). Estimation of tree heights and stand volume using an airborne lidar system. *Remote Sensing of environment, 56*, 1-7

Noest, A.J. (1994). Neural processing of overlapping shapes. *Shape in Picture* (pp. 383-392): Springer

Nowak, D.J., Crane, D.E., & Stevens, J.C. (2006). Air pollution removal by urban trees and shrubs in the United States. *Urban Forestry & Urban Greening, 4*, 115-123

Ørka, H.O., Næsset, E., & Bollandsås, O.M. (2009). Classifying species of individual trees by intensity and structure features derived from airborne laser scanner data. *Remote Sensing of environment, 113*, 1163-1174

Osada, R., Funkhouser, T., Chazelle, B., & Dobkin, D. (2002). Shape distributions. *ACM Transactions on Graphics (TOG), 21*, 807-832

Pataki, D.E., Carreiro, M.M., Cherrier, J., Grulke, N.E., Jennings, V., Pincetl, S., Pouyat, R.V., Whitlow, T.H., & Zipperer, W.C. (2011). Coupling biogeochemical cycles in urban environments: ecosystem services, green solutions, and misconceptions. *Frontiers in Ecology and the Environment, 9*, 27-36

Persson, A., Holmgren, J., & Sv∂derman, U. (2002a). Detecting and measuring individual trees using an airborne laser scanner. *Photogrammetric Engineering and Remote Sensing, 68*, 925-932

Persson, A., Holmgren, J., & Söderman, U. (2002b). Detecting and measuring individual trees using an airborne laser scanner. *Photogrammetric Engineering and Remote Sensing, 68*, 925-932

Petropoulos, G.P., Arvanitis, K., & Sigrimis, N. (2012a). Hyperion hyperspectral imagery analysis combined with machine learning classifiers for land use/cover mapping. *Expert systems with Applications, 39*, 3800-3809

Plourde, L.C., Ollinger, S.V., Smith, M.-L., & Martin, M.E. (2007). Estimating species abundance in a northern temperate forest using spectral mixture analysis. *Photogrammetric Engineering & Remote Sensing, 73*, 829-840

Pohl, C., & Van Genderen, J.L. (1998). Review article multisensor image fusion in remote sensing: concepts, methods and applications. *International Journal of Remote Sensing, 19*, 823-854

Poland, T.M., & McCullough, D.G. (2006). Emerald ash borer: invasion of the urban forest and the threat to North America's ash resource. *Journal of Forestry, 104*, 118-124

Pontius, J., Martin, M., Plourde, L., & Hallett, R. (2008). Ash decline assessment in emerald ash borer-infested regions: A test of tree-level, hyperspectral technologies. *Remote Sensing of environment, 112*, 2665-2676

Popescu, S., Wynne, R., & Nelson, R. (2000). Estimating forest vegetation biomass using airborne LIDAR measurements. In, *Proceedings of the second conference on geospatial information in agriculture and forestry, 10-12 January 2000, Lake Buena Vista, Florida, USA* (pp. 346-353)

Popescu, S.C. (2007). Estimating biomass of individual pine trees using airborne lidar. *Biomass and Bioenergy, 31*, 646-655

Popescu, S.C., & Wynne, R.H. (2004). Seeing the Trees in the Forest: Using Lidar and Multispectral Data Fusion with Local Filtering and Variable Window Size for Estimating Tree Height. *Photogrammetric Engineering & Remote Sensing, 70*, 589-604

Popescu, S.C., Wynne, R.H., & Nelson, R.F. (2002). Estimating plot-level tree heights with lidar: local filtering with a canopy-height based variable window size. *Computers and electronics in agriculture, 37*, 71-95

Popescu, S.C., Wynne, R.H., & Nelson, R.F. (2003). Measuring individual tree crown diameter with lidar and assessing its influence on estimating forest volume and biomass. *Canadian journal of remote sensing, 29*, 564-577

Proietti, P., Sdringola, P., Brunori, A., Ilarioni, L., Nasini, L., Regni, L., Pelleri, F., Desideri, U., & Proietti, S. (2016). Assessment of carbon balance in intensive and extensive tree cultivation systems for oak, olive, poplar and walnut plantation. *Journal of Cleaner Production, 112*, 2613-2624

Pugh, S.A., Liebhold, A.M., & Morin, R.S. (2011). Changes in ash tree demography associated with emerald ash borer invasion, indicated by regional forest inventory data from the Great Lakes States. *Canadian Journal of Forest Research, 41*, 2165-2175

Quintano, C., Fernández-Manso, A., & Roberts, D.A. (2013). Multiple Endmember Spectral Mixture Analysis (MESMA) to map burn severity levels from Landsat images in Mediterranean countries. *Remote Sensing of environment, 136*, 76-88

Roberts, D.A., Gardner, M., Church, R., Ustin, S., Scheer, G., & Green, R. (1998). Mapping chaparral in the Santa Monica Mountains using multiple endmember spectral mixture models. *Remote Sensing of environment, 65*, 267-279

San Souci, J., Hanou, I., & Puchalski, D. (2009). High-resolution remote sensing image analysis for early detection and response planning for emerald ash borer. *Photogrammetric Engineering & Remote Sensing*, 905

Shang, X., & Chisholm, L.A. (2014). Classification of Australian native forest species using hyperspectral remote sensing and machine-learning classification algorithms. *Selected Topics in Applied Earth Observations and Remote Sensing, IEEE Journal of, 7*, 2481-2489

Sheng, Y., Gong, P., & Biging, G. (2001). Model-based conifer-crown surface reconstruction from high-resolution aerial images. *Photogrammetric Engineering and Remote Sensing, 67*, 957-966

Singh, K.K., Vogler, J.B., Shoemaker, D.A., & Meentemeyer, R.K. (2012). LiDAR-Landsat data fusion for large-area assessment of urban land cover: Balancing spatial resolution, data volume and mapping accuracy. *ISPRS Journal of Photogrammetry and Remote Sensing, 74*, 110-121

Sinha, S., Bhola, A., Panchal, V., Singhal, S., & Abraham, A. (2012). Resolving mixed pixels by hybridization of biogeography based optimization and ant colony optimization. In, *2012 IEEE Congress on Evolutionary Computation* (pp. 1-6): IEEE

Sivyer, D. (2010). Mapping the future for EAB readiness and response planning in Milwaukee. *Forestry Source, 15*

Somers, B., Cools, K., Delalieux, S., Stuckens, J., Van der Zande, D., Verstraeten, W.W., & Coppin, P. (2009). Nonlinear hyperspectral mixture analysis for tree cover estimates in orchards. *Remote Sensing of environment, 113*, 1183-1193

Somers, B., Verbesselt, J., Ampe, E.M., Sims, N., Verstraeten, W.W., & Coppin, P. (2010). Spectral mixture analysis to monitor defoliation in mixed-aged Eucalyptus globulus Labill plantations in southern Australia using Landsat5-TM and EO-1Hyperion data. *International Journal of Applied Earth Observation and Geoinformation, 12*, 270-277

Song, J.-H., Han, S.-H., Yu, K., & Kim, Y.-I. (2002). Assessing the possibility of land-cover classification using lidar intensity data. *International archives of photogrammetry remote sensing and spatial information sciences, 34*, 259-262

St-Onge, B., Jumelet, J., Cobello, M., & Véga, C. (2004). Measuring individual tree height using a combination of stereophotogrammetry and lidar. *Canadian Journal of Forest Research, 34*, 2122-2130

Tao, S., Guo, Q., Li, L., Xue, B., Kelly, M., Li, W., Xu, G., & Su, Y. (2014). Airborne Lidar-derived volume metrics for aboveground biomass estimation: A comparative assessment for conifer stands. *Agricultural and forest meteorology, 198*, 24-32

Ustin, S., & Xiao, Q. (2001). Mapping successional boreal forests in interior central Alaska. *International Journal of Remote Sensing, 22*, 1779-1797

Van Leeuwen, M., Coops, N.C., & Wulder, M.A. (2010). Canopy surface reconstruction from a LiDAR point cloud using Hough transform. *Remote Sensing Letters, 1*, 125-132

Verma, A., & Kumar, A. (2011). Design of low-pass filters using some defected ground structures. *AEU-International Journal of Electronics and Communications, 65*, 864-872

Voss, M., & Sugumaran, R. (2008). Seasonal effect on tree species classification in an urban environment using hyperspectral data, LiDAR, and an object-oriented approach. *Sensors, 8*, 3020-3036

Wang, C., & Glenn, N.F. (2008). A linear regression method for tree canopy height estimation using airborne lidar data. *Canadian journal of remote sensing, 34*, S217-S227

Wang, Y., & Jarvis, P. (1990). Influence of crown structural properties on PAR absorption, photosynthesis, and transpiration in Sitka spruce: application of a model (MAESTRO). *Tree physiology, 7*, 297-316

Whitney, G.G., & Upmeyer, M.M. (2004). Sweet trees, sour circumstances: The long search for sustainability in the North American maple products industry. *Forest Ecology and Management, 200*, 313-333

Wu, B., Yu, B., Wu, Q., Huang, Y., Chen, Z., & Wu, J. (2016). Individual tree crown delineation using localized contour tree method and airborne LiDAR data in coniferous forests. *International Journal of Applied Earth Observation and Geoinformation, 52*, 82-94

Wu, C. (2004). Normalized spectral mixture analysis for monitoring urban composition using ETM+ imagery. *Remote Sensing of environment, 93*, 480-492

Wu, C., & Murray, A.T. (2003). Estimating impervious surface distribution by spectral mixture analysis. *Remote Sensing of environment, 84*, 493-505

Wu, C., Niu, Z., Tang, Q., & Huang, W. (2008). Estimating chlorophyll content from hyperspectral vegetation indices: Modeling and validation. *Agricultural and forest meteorology, 148*, 1230-1241

Wulder, M., Niemann, K.O., & Goodenough, D.G. (2000). Local maximum filtering for the extraction of tree locations and basal area from high spatial resolution imagery. *Remote Sensing of environment, 73*, 103-114

Wulder, M.A., White, J.C., Nelson, R.F., Næsset, E., Ørka, H.O., Coops, N.C., Hilker, T., Bater, C.W., & Gobakken, T. (2012). Lidar sampling for large-area forest characterization: A review. *Remote Sensing of environment, 121*, 196-209

Xiao, Q., Ustin, S., & McPherson, E. (2004). Using AVIRIS data and multiple-masking techniques to map urban forest tree species. *International Journal of Remote Sensing, 25*, 5637-5654

Yao, X., Titus, S.J., & MacDonald, S.E. (2001). A generalized logistic model of individual tree mortality for aspen, white spruce, and lodgepole pine in Alberta mixedwood forests. *Canadian Journal of Forest Research, 31*, 283-291

Yu, Q., Gong, P., Clinton, N., Biging, G., Kelly, M., & Schirokauer, D. (2006). Object-based detailed vegetation classification with airborne high spatial resolution remote sensing imagery. *Photogrammetric Engineering & Remote Sensing, 72*, 799-811

Yu, Y., Saatchi, S., Heath, L.S., LaPoint, E., Myneni, R., & Knyazikhin, Y. (2010). Regional distribution of forest height and biomass from multisensor data fusion. *Journal of Geophysical Research: Biogeosciences, 115*

Zeide, B., & Pfeifer, P. (1991). A method for estimation of fractal dimension of tree crowns. *Forest Science, 37*, 1253-1265

Zhang, C., & Qiu, F. (2012). Mapping individual tree species in an urban forest using airborne lidar data and hyperspectral imagery. *Photogrammetric Engineering & Remote Sensing, 78*, 1079-1087

Zhao, D., Pang, Y., Li, Z., & Sun, G. (2013). Filling invalid values in a lidar-derived canopy height model with morphological crown control. *International Journal of Remote Sensing, 34*, 4636-4654

CURRICULUM VITAE

Haijian Liu

EDUCATION

2017.5. Ph.D. Geography, University of Wisconsin-Milwaukee, USA

Dissertation title: Ash Tree Identification Based on the Integration of Hyperspectral Imagery and High-Density LiDAR Data

2013.5. M.S. Geography, University of North Texas, USA

Thesis title: Automated Treetop Detection and Tree Crown Identification Using Discrete Return LiDAR Data.

1999. 7. B.S. Civil Engineer, University of Electronic Science and Technology of China, China

PUBLICATIONS

1. Liu, H., and Wu, C. (2016). Tree Crown Estimation, Using Discrete Airborne LiDAR Data. *Canadian Journal of Remote Sensing*, 42(5): 610-618.

2. Liu, H., and Dong, P. (2014). A New Method of Generating Canopy Height Models from Discrete-Return LiDAR Point Clouds. *Remote Sensing Letters*, 5(6):575-582.